v. 3, n. 20, 2023

Journal of
Engineering
Research

INVESTIGATING THE INTERFERENCE FIT REQUIREMENTS FOR CUSTOMIZED DUAL-FIT FASTENERS IN A LINEAR GUIDE RAIL MOUNTING APPLICATION

William Manjud Maluf Filho
Fatec Mauá, Mechanical Manufacturing Technology professor, Mauá – SP, Brazil
https://lattes.cnpq.br/9888914170875821

Allan Henrique Silva
Fatec Mauá, Mechanical Manufacturing Technology student, Mauá – SP, Brazil

João Felipe de Souza Lourenço
Centro Universitário FEI, Mechanical Engineering student, São Bernardo do Campo – SP, Brazil
https://www.linkedin.com/in/jo%C3%A3o-felipe-de-souza-louren%C3%A7o-72a3a0139

Luís Américo Alves dos Santos
Fatec Mauá, Mechanical Manufacturing Technology student, Mauá – SP, Brazil
https://www.linkedin.com/in/luis-americo-446b44266

Willian da Silva Santos
Fatec Mauá, Mechanical Manufacturing Technology student, Mauá – SP, Brazil

Abstract: This article investigates the interference fit requirements for customized dual-fit fasteners in a linear guide rail mounting application. The shaft support mount used in this study is designed to support linear guide rails and is fixed to a surface using customized dual-fit fasteners. The interference fit between the two parts of fasteners is calculated to determine the necessary friction to hold both parts attached. This study aims to optimize the frictional force in the shaft support mount attachment and investigates the effects of the fastener diameter, material, and surface roughness on the interference fit. The results of this study show that the interference fit between the two parts of the fasteners significantly affects the frictional force required to hold the shaft support mount attached to the surface. The findings of this research can be used to improve the design of linear guide rail mounting systems and provide guidance for engineers and designers when selecting customized dual-fit fasteners for similar applications.
Keywords: Interference fit; Customized dual-fit fasteners; Linear guide rails; Shaft support mount; Frictional force optimization.

INTRODUCTION

In mechanical engineering, linear guide rails are commonly used in a wide range of applications to support and guide moving parts with high precision. One critical aspect of linear guide rail design is the attachment of the shaft support mounts to the surface. In order to achieve the desired stability and accuracy of the system, the shaft support mount must be securely fastened to the surface in a way that can withstand the forces and loads applied during operation.

One popular method for attaching shaft support mounts to surfaces is through the use of fasteners such as screws or bolts. However, these types of fasteners can be cumbersome to use and may not always provide the necessary level of stability and accuracy required for certain applications. As an alternative, customized dual-fit fasteners can be used to attach shaft support mounts to surfaces. Customized dual-fit fasteners consist of two tailored parts that are connected through an interference fit, providing a secure and reliable attachment method without the need for traditional fasteners.

In this study, we investigate the interference fit requirements for customized dual-fit fasteners in a linear guide rail mounting application. Specifically, we aim to determine the optimal interference fit between the two parts of the tailored bipartite pin in order to achieve the necessary frictional force to hold the shaft support mount attached to the surface. By doing so, we hope to provide important insights into the use of tailored bipartite fastening pins in linear guide rail mounting applications and inform the development of more efficient and effective mounting systems.

This article is organized into six sections, five of which are numbered and one of which is the reference list. The sections are outlined below.

a) Section 1 – Introduction: in this section, we provide an overview of the background and context of the study, including a discussion of the importance of secure attachment methods for linear guide rail mounting applications. We also introduce the use of tailored bipartite fastening pins as an alternative to traditional fasteners and outline the specific objectives of the study.

b) Section 2 – Literature Review: in this section, we review the existing literature on linear guide rail mounting methods and the use of tailored bipartite fastening pins. We discuss previous studies that have investigated the use of fasteners

in similar applications and review the relevant theories and concepts related to interference fit.

c) Section 3 – Materials and Methods: in this section, we describe the materials and methods used in the study. We provide details on the geometry and material properties of the shaft support mount and the surface it will be attached to. We also outline the specific operational conditions that the setup will experience to determine the necessary interference fit between the two parts of the tailored bipartite fastening pin.

d) Section 4 – Results and Discussions: in this section, we discuss the optimal interference fit between the two parts of the tailored bipartite fastening pin and compare our findings to existing theories and models. We also discuss the implications of our results for the design and development of linear guide rail mounting systems.

e) Section 5 – Conclusions: in this section, we summarize the main findings of the study and discuss their significance. We highlight the advantages of using tailored bipartite fastening pins for linear guide rail mounting applications and emphasize the importance of proper interference fit in achieving secure and stable attachments. We also suggest directions for future research in this area.

f) References: finally, we provide a list of references used in the study, including previous studies on linear guide rail mounting and tailored bipartite fastening pins, as well as relevant theories and concepts.

LITERATURE REVIEW

To conduct the literature review for this study, several authoritative sources were consulted, including well-known machine design textbooks and academic journals available in online databases. Some of the databases consulted include Elsevier, ScienceDirect, IEEE Xplore, Springer, and ASME Digital Collection. In addition, various search engines, such as Google Scholar, were utilized to identify relevant publications. The literature review process was enhanced by the use of artificial intelligence tools, which enabled the quick and efficient sorting of articles based on their relevance to the study. The use of these tools also facilitated the organization and synthesis of information during the writing of the paper.

LINEAR GUIDE RAILS

Linear guides are believed to have been utilized since ancient Egypt, but it wasn't until 1932 when the modern linear guide was patented. The first rolling elements used in the linear guide were made from steel due to its ability to provide precise and smooth linear motion. Thomson Linear, a US company, introduced the first recirculation ball in their ball screws in 1946, marking a significant advancement in the technology. Over time, companies continued to improve and innovate the linear guide, leading to the highly refined and widely used product we have today.

Linear guide rails are mechanical components commonly used in various industrial applications, such as manufacturing and automation. These rails are designed to support and guide linear motion along a specific path, typically in a straight line. They consist of a rail and a carriage that moves along the rail, and they can be found in various configurations, such as single or multiple rails, and with different types of carriages, such as ball or roller bearings. Linear guide rails offer several advantages, such as high precision, smooth and quiet operation, and high load capacity, making them ideal for use

in applications where precision and smooth motion are required. They are widely used in CNC machines, robotics, semiconductor manufacturing equipment, and other precision machinery applications (GROSS *et al.*, 2013).

There are several types of linear guide rails, including:

a) Ball-type linear guide rails: This type of linear guide rail uses recirculating ball bearings to provide smooth and accurate linear motion. An example is shown in Figure 1.

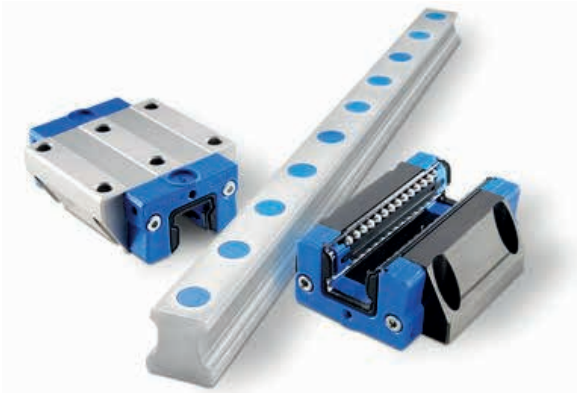

Figure 1 - 500 series ball linear guide by Thomson (https://www.thomsonlinear.com/en/products/profile-rail/500-series-ball-guide#products)

b) Roller-type linear guide rails: This type of linear guide rail uses rollers instead of balls to provide linear motion. Roller guide rails can handle heavier loads than ball guide rails. An example is shown in Figure 2.

Figure 2 - 500 series roller linear guide by Thomson (https://www.thomsonlinear.com/en/products/profile-rail/500-series-roller-guide#products)

c) Plain linear guide rails: This type of linear guide rail is made from a simple sliding surface that provides linear motion with low friction. An example is show in Figure 3.

Figure 3 - Linear guide by HepcoMotion (https://www.hepcomotion.com/product/linear-guides/mini-rail-miniature-linear-guides/)

d) Magnetic linear guide rails: This type of linear guide rail uses magnets to provide non-contact linear motion with zero friction. An example is shown in Figure 4.

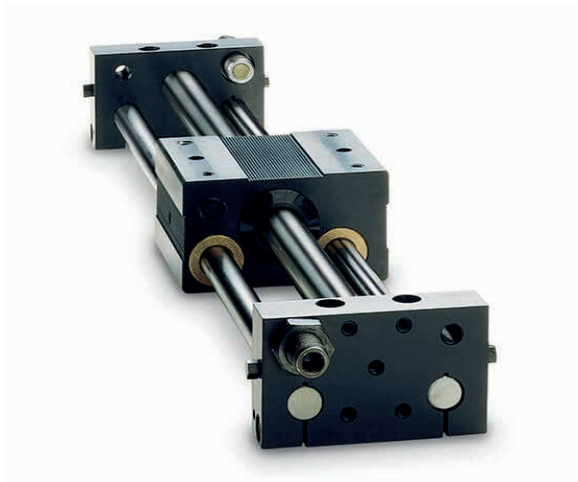

Figure 4 - MGS magnetic linear slides by Tolomatic (https://www.tolomatic.com/products/product-details/mgs-magnetic-linear-slides/)

e) Air bearing linear guide rails: This type of linear guide rail uses a thin layer of compressed air to provide linear motion with extremely low friction. An example is shown in Figure 5.

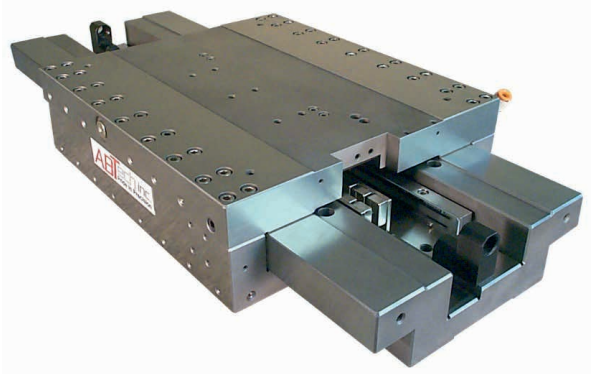

Figure 5 - Air-bearing linear stages by ABTech (https://abtechmfg.com/precision-motion-components/linear-stages/air-bearing-linear-stages/)

f) Hydrostatic linear guide rails: This type of linear guide rail uses a thin layer of oil or another fluid to provide linear motion with extremely low friction. An example is shown in Figure 6.

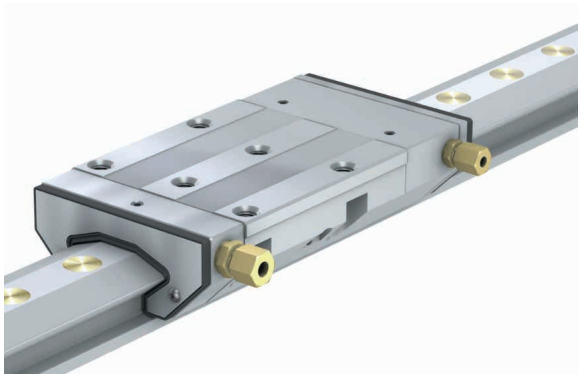

Figure 6 - Hydrostatic compact guidance system by Schaeffler (https://www.schaeffler.com/remotemedien/media/_shared_media/05_products_services/linear_guidance_systems/monorail_guidance_systems/00016D9C.jpg)

Collins (2015) discusses three important factors to consider when mounting linear guide rails. Firstly, it emphasizes the need to ensure that the mounting surfaces are clean, flat, and parallel. Any variation in the surface can result in misalignment, which can significantly impact the performance of the guide rails. Secondly, the article highlights the importance of appropriate fastening torque. Over-tightening can cause deformation, while under-tightening can result in the guide rails coming loose. Finally, it stresses the significance of ensuring proper lubrication of the guide rails. Insufficient lubrication can cause increased friction and wear, while excessive lubrication can result in contamination and reduce the effectiveness of the lubricant. The article concludes by reminding readers that by paying attention to these three factors, they can ensure optimal performance and longevity of their linear guide rails.

LINEAR GUIDE RAILS APPLICATIONS

Wei *et al.* (2021) discuss the establishment of a static precise finite element model for the rolling linear guide (RLG) using the Hertz theory and finite element method (FEM). The

article describes the specific modeling process of the overall and unit slice finite element models of the RLG and provides comparative analysis results. The article also studies the mapping laws between external load, preload value, curvature ratio, carriage's wall thickness, guide's width, and static mechanical properties of RLG. The combined application of these precise finite element models can solve the problems of large calculation and low efficiency in statics of RLG and provides a new way to achieve high-efficiency and high-rigidity design of RLG from the source.

Chang and Hung (2014) present an analytical and finite element (FE) modeling approach for analyzing the dynamic behavior of a linear feeding stage with different arrangements of rolling guides. The analytical model is developed based on the transfer matrix method, which considers the stiffness and damping of the components in the system. The FE model is established to verify the analytical model and provide more detailed information about the dynamic behavior. The effects of different guide arrangements, including parallel, diagonal, and hybrid arrangements, on the natural frequency, damping ratio, and mode shapes of the feeding stage are investigated. The results show that the diagonal arrangement has the highest natural frequency and the lowest damping ratio, while the hybrid arrangement has the lowest natural frequency and the highest damping ratio. The analytical and FE modeling approach can provide insights into the dynamic behavior of linear feeding stages and assist in the design and optimization of these systems.

Song *et al.* (2018) present an improved design of a roller linear guide for heavy load applications. The authors used finite element analysis (FEA) and measurement techniques to identify the weak points of the original design, and proposed a modified design that improves the guide's load capacity and stiffness. The FEA results showed that the new design reduces the stress concentration in the critical areas of the guide, resulting in a significant increase in load capacity. The authors also performed a series of tests on the new design, and the experimental results confirmed the effectiveness of the proposed modifications. Overall, this study demonstrates the importance of using FEA and measurement techniques to improve the design of roller linear guides for heavy load applications.

Sun *et al.* (2013) present a precise finite element model for the dynamics analysis of linear rolling guide. The study focuses on the supporting direction of the linear guide, where an elastic foundation model is used to simulate the supporting condition. The model is established based on Hertz contact theory and finite element method (FEM). The analysis considers the effects of load, speed, and stiffness on the dynamic performance of the linear guide. The results show that the proposed model can accurately predict the dynamic behavior of the guide and is suitable for analyzing the dynamic characteristics of rolling guides.

Shaukharova *et al.* (2021) present a study on the stiffness of linear guide pairs by both experimental and finite element analysis (FEA) methods. The stiffness of the guide pairs was measured experimentally by applying different loads on the carriage and measuring the corresponding displacement. The FEA model was developed using ANSYS software and validated by comparing the results with the experimental data. The effects of preload, length, and mounting method on the stiffness of the guide pairs were investigated. The results showed that the stiffness of the guide pairs increased with preload and length, and that the mounting method had a significant effect on the stiffness. The study provides useful insights into the design and optimization of

linear guide pairs for various applications.

Rommers *et al.* (2022) propose a new type of flexure-based linear guide with torsion reinforcement structures. The guide consists of three parts: the base, the slider, and the flexure mechanism. The flexure mechanism is designed to be preloaded in all directions to ensure that the slider is stable and to minimize the frictional resistance. The torsion reinforcement structures are used to enhance the torsional stiffness of the guide, which is crucial for precision positioning applications. The authors conducted finite element analysis and experimental tests to evaluate the performance of the guide. The results show that the proposed guide has a higher stiffness than conventional flexure-based guides, and it is suitable for high-precision linear motion control applications.

Nguyen *et al.* (2022) present an optimization design approach for a compliant linear guide (CLG) that achieves high-precision feed drive mechanisms. The authors used a simplified beam model of the CLG to determine its mechanical behavior. An analytical model was developed to estimate the stress and deformation of the CLG under different load and geometric conditions. The results of the model were validated using finite element analysis (FEA) simulations. The authors then used a particle swarm optimization (PSO) algorithm to optimize the design parameters of the CLG to minimize its maximum stress and maximize its natural frequency. The proposed approach was demonstrated to be effective in optimizing the CLG design for high-precision feed drive mechanisms. The results show that the optimized CLG has a higher natural frequency and lower maximum stress compared to the original design.

Sa'diyah *et al.* (2021) present a design approach for the ballscrew linear guide actuator used in an earthquake shaking table (EST). The actuator's design is optimized using finite element analysis (FEA) and a neural network model. The neural network model is used to predict the performance of the actuator based on various design parameters, such as the diameter and pitch of the ballscrew, the length and width of the linear guide, and the size of the motor. The FEA is used to verify the performance of the optimized design and to ensure that the actuator can withstand the high forces and accelerations required for EST testing. The proposed design approach is shown to be effective in improving the performance and reliability of the EST actuator.

Shih *et al.* (2021) propose a method to monitor the preload variation of a linear guide positioning stage using artificial neural networks (ANNs). The authors developed a numerical model of the linear guide stage with various preload values, and the corresponding displacement data was collected. The ANNs were then trained using the displacement data to predict the preload variation of the linear guide stage. The proposed method was validated experimentally, and the results showed that the ANN-based approach can accurately predict the preload variation of the linear guide stage. The proposed method has potential applications in real-time monitoring and control of precision positioning systems.

Liu *et al.* (2021a) present numerical model to study the nonlinear dynamics of the linear guide slide platform taking into account the assembly error. The model includes a geometric error and a material nonlinearity of the guide rail. The governing equations are solved using the fourth-order Runge-Kutta method. The results show that the nonlinear dynamics of the system are influenced by the assembly error, which causes the vibration amplitude of the platform to increase significantly. The research provides useful information for improving the performance of the linear guide slide platform and reducing

the impact of assembly error.

Liu *et al.* (2021b) presents a system for straightening linear guide rails. The system consists of a straightening machine, a measuring system, and a control system. The measuring system uses laser displacement sensors to measure the deflection of the rail, and the control system uses a proportional-integral-derivative (PID) controller to adjust the straightening machine to correct the deflection. The article describes the design and implementation of the system and presents experimental results showing that the system can effectively straighten a curved rail to within a specified tolerance. The system has potential applications in the manufacturing and maintenance of high-precision equipment that relies on straight guide rails.

Liu and Hao (2022) propose a new cylindrical compliant linear guide with decoupling parallelogram mechanisms that can achieve a high precision and stiffness. The design of the guide is based on the concept of compliant mechanisms, which eliminates the need for traditional bearings and reduces the complexity of the mechanism. The article describes the design process, including the analytical modeling and finite element analysis of the guide's performance. The experimental results show that the proposed guide has a high precision and stiffness and can achieve a stroke of up to 5mm. The guide is also compact and easy to assemble, making it suitable for various precision engineering applications.

Krampert *et al.* (2021a) describe a novel technique for measuring localized surface strain on a linear guide using diamond-like carbon (DLC) coating. The authors applied DLC coating on the guide rail and measured the changes in its surface strain caused by load variations. They found that the surface strain changed linearly with the applied load, allowing for accurate load measurements. The authors also developed a finite element model to validate the experimental results. This technique has the potential to be used in various applications where accurate load measurement is required.

Krampert *et al.* (2021b) investigate the stiffness hysteresis of profiled rail guides and its impact on the accuracy of machine tools. The authors present experimental results on the stiffness hysteresis of profiled rail guides and analyze the causes of the phenomenon. They also propose a mathematical model to describe the stiffness hysteresis and validate it with experimental data. The results show that the stiffness hysteresis is caused by the elastic deformation and sliding friction of the contact surfaces between the guide and the carriage. The mathematical model can accurately describe the stiffness hysteresis phenomenon, and the proposed compensation method can effectively reduce the influence of stiffness hysteresis on the accuracy of machine tools.

Li *et al.* (2021) propose a new error equivalence model for the kinematic error of the linear axis of high-end machine tools. The study first analyzes the characteristics of the traditional error equivalence model and proposes a new error equivalence model based on the concept of equivalent homogeneous strain. The new model is applied to analyze the kinematic error of a linear axis of a high-end machine tool, and the results show that the model can effectively predict the kinematic error of the linear axis. The proposed model can be used for the design and optimization of linear axes in high-end machine tools, contributing to the improvement of machining accuracy and productivity.

In chapter 5 of their book, Collins *et al.* (2009) describe an electronic detector package used in a high-speed paper mill to monitor paper thickness. The detector package moves along horizontal precision guide rails that are solidly supported at 24-

inch intervals. The package must not exceed a vertical displacement of 0.005 inches during the scanning process to obtain acceptable thickness measurements. The total weight of the detector package is 400 lbs, and each of the two guide rails is a solid AISI 1020 cold-drawn steel cylindrical bar with a diameter of 1.0000 inches. The support rails are modeled as a beam with fixed ends and a midspan concentrated load, and half of the detector weight is supported by each rail. A simplified sketch is shown in Figure 7.

In chapter 20 of their book, Collins *et al.* (2009) discusse the need for a sheet-thickness measurement and control system to maintain a nominal target thickness of t=0.010 inch with a tolerance of 10% across a production width of 20 feet for specialized "sheet goods" production. The proposed system involves an on-line scanning sensor package tied to a computer-controlled aperture-adjustment device. The sensor package consists of an upper and lower carriage unit with a clearance space of approximately 0.040 inch between their sensor faces to allow continuous non-contacting passage of the sheet goods. The fully instrumented upper and lower carriage units weigh about 50 pounds each. The article also discusses the need for special high-precision support rails and rollers and a laser-based alignment procedure to ensure vertical position accuracy of the moving sensors to within 0.0005 inch, if the support rails are solidly mounted to the frame. A sketch is shown in Figure 8.

Here is an important additional point to consider regarding linearly-guided systems and precise constraints: When linear systems are rigidly guided on two separate axes, they become over-constrained. This can result in issues such as jamming, sticking, increased wear, and difficulties in manufacturing. Finding solutions for these problems may not be straightforward and often involves making challenging decisions, such as eliminating the fixed center-to-center distance in either the carriage or the rails. Failing to address these issues can lead to troublesome consequences (SKAKOON, 2008). An example of poor design for linearly-guided systems is shown in Figure 9.

The RoundRail Linear Guides and Components document published by Thomsonlinear (2023) showcases several applications of linear guides and their structures. A cam-actuated part transfer mechanism is shown in Figure 10.

Accurately position an inspection probe of an X-Y system over small electronic components could be accomplished by the mechanism shown in Figure 11.

Reduce deflection of plate loader to minimize scrap and improve cycle speed could be done by the equipment shown in Figure 12.

Redesign a wire straightening/feeding mechanism for a wire drawing machine that improves cycle time and minimizes downtime could be accomplished by the equipment shown in Figure 13.

It is possible to build an X-Y system that transfers the work piece between two separate machining stations such as the mechanism shown in Figure 14.

DETACHABLE FASTENINGS

Detachable fastenings, as the name suggests, are mechanical connections that allow for the easy and convenient removal or separation of two or more components. These fastenings are designed to provide a secure attachment while also enabling disassembly or reassembly when needed. They are commonly used in various industries and applications where frequent assembly, maintenance, or repair is required (JIANG, 2019).

There are several types of detachable fastenings, each with its unique characteristics and applications. Some of the commonly used

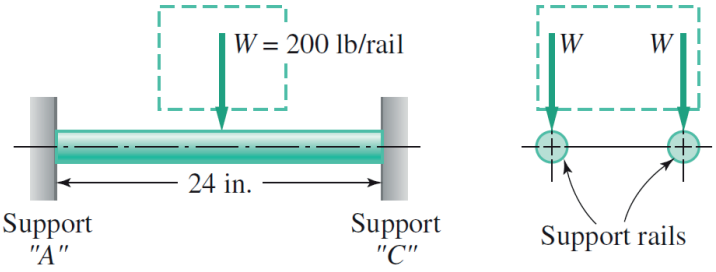

Figure 7 - Simplified sketch of thickness-measuring scanner for paper mill application (COLLINS *et al.*, 2009)

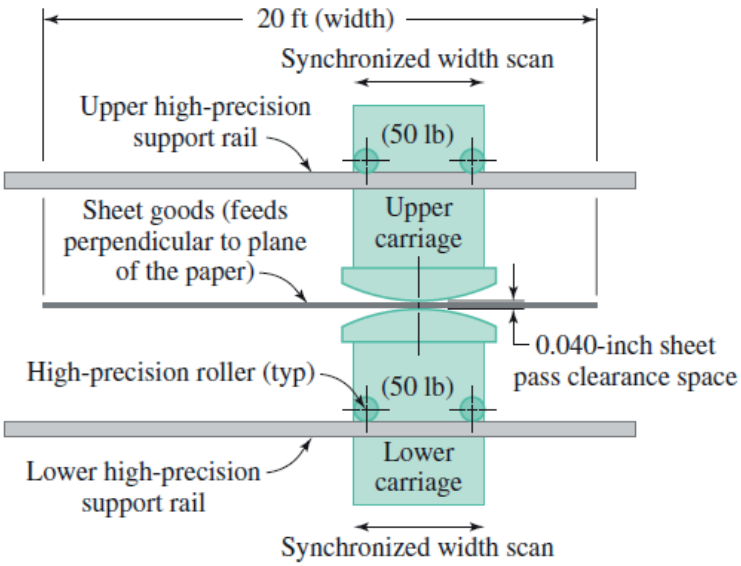

Figure 8 - Sketch showing the proposed thickness measurement system for continuous production of 20-foot-wide special sheet goods (COLLINS *et al.*, 2009)

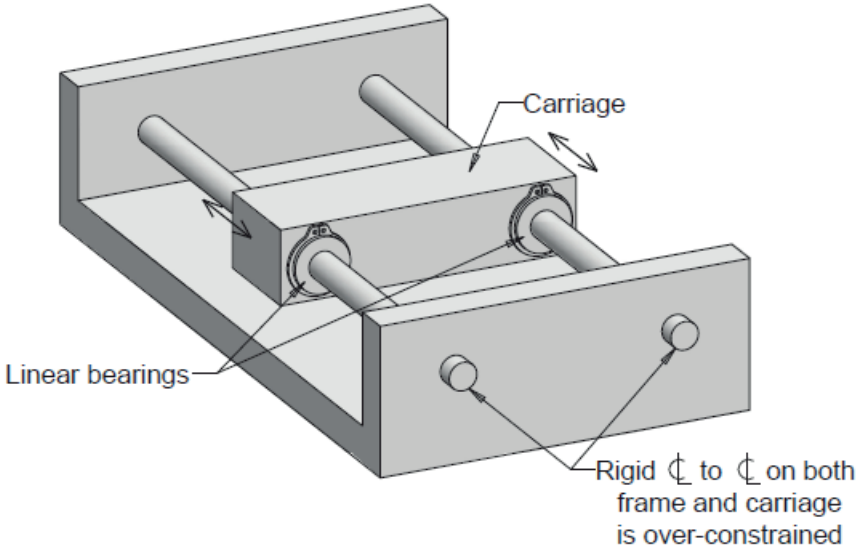

Figure 9 - The center- to-center distance is fully constrained two different ways, giving over-constraint (SKAKOON, 2008)

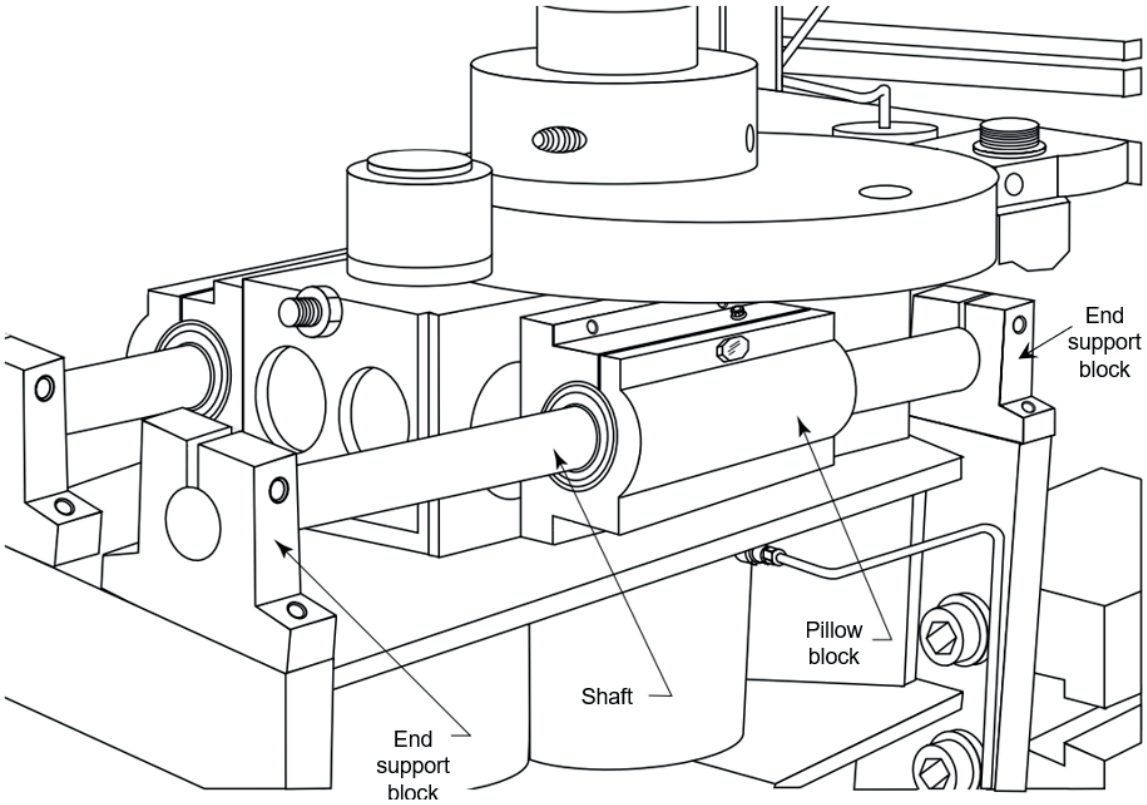

Figure 10 - Cam-actuated part transfer mechanism for multiple-transfer press (THOMSONLINEAR, 2023)

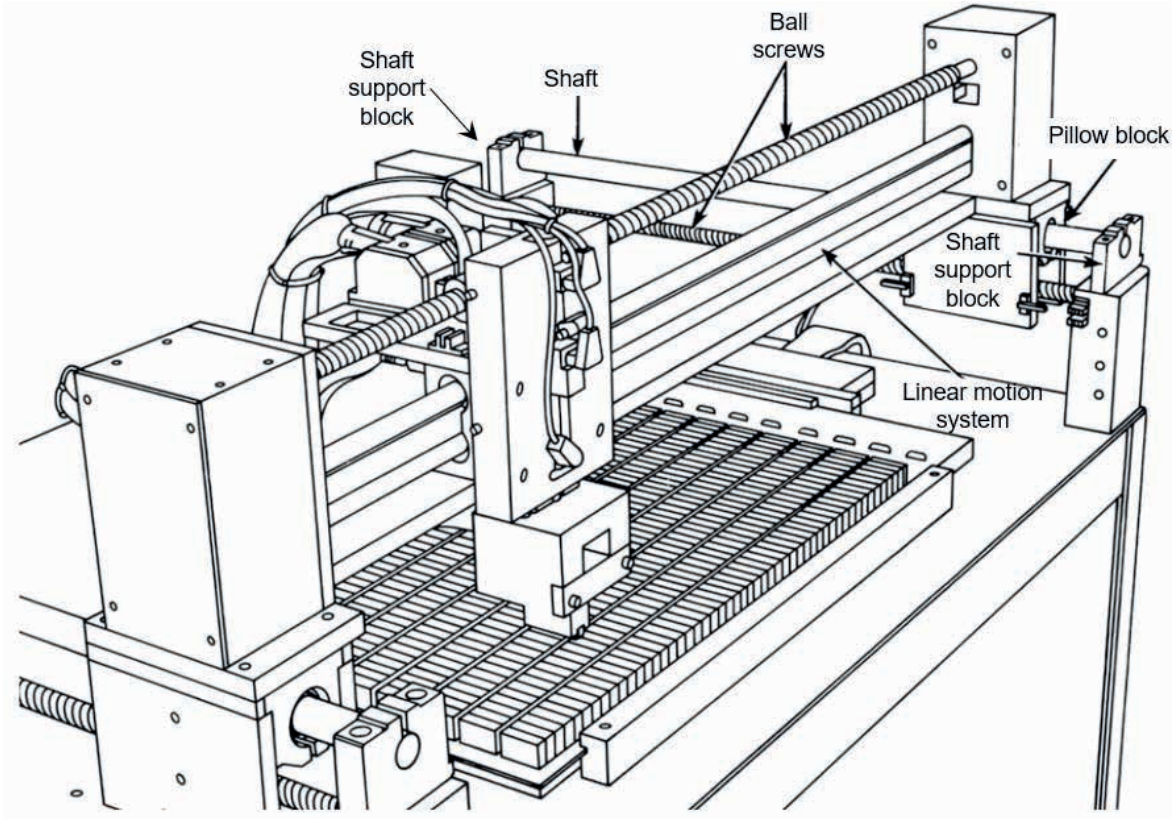

Figure 11 - Inspection system (THOMSONLINEAR, 2023)

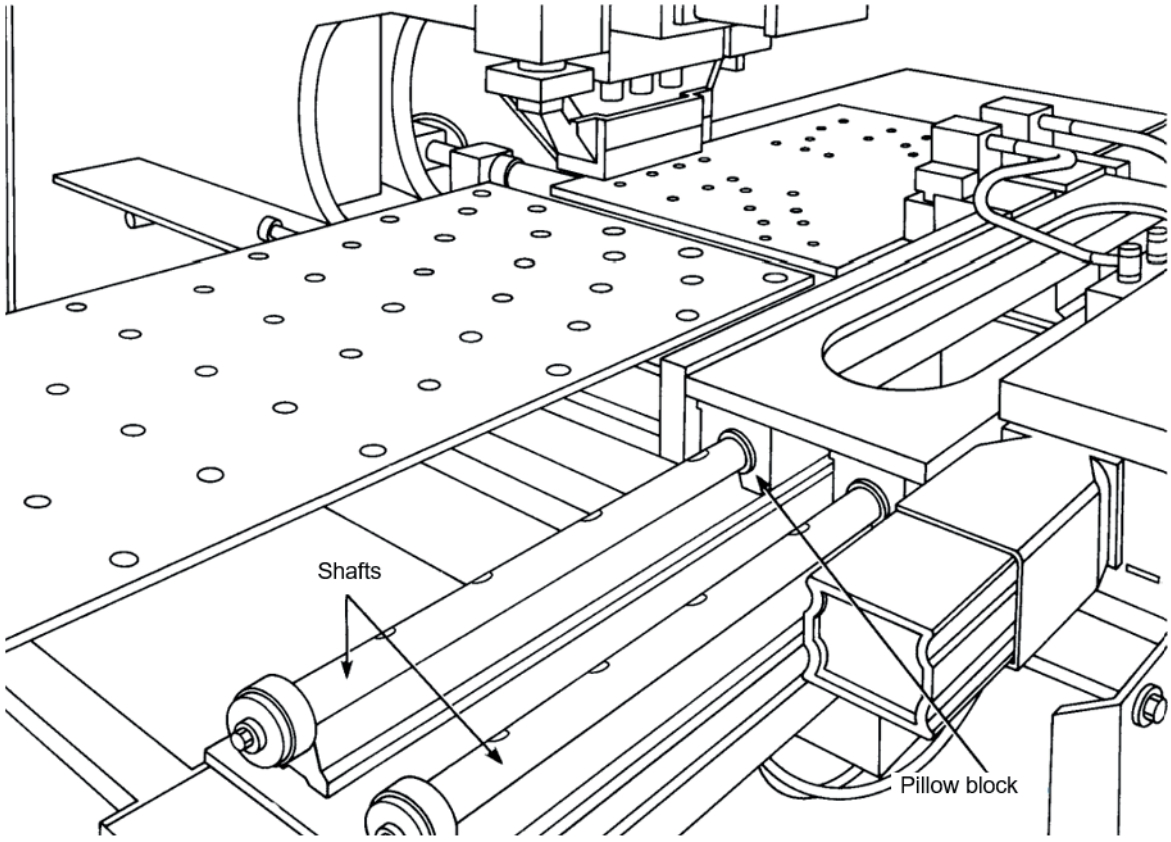

Figure 12 - Punch press (THOMSONLINEAR, 2023)

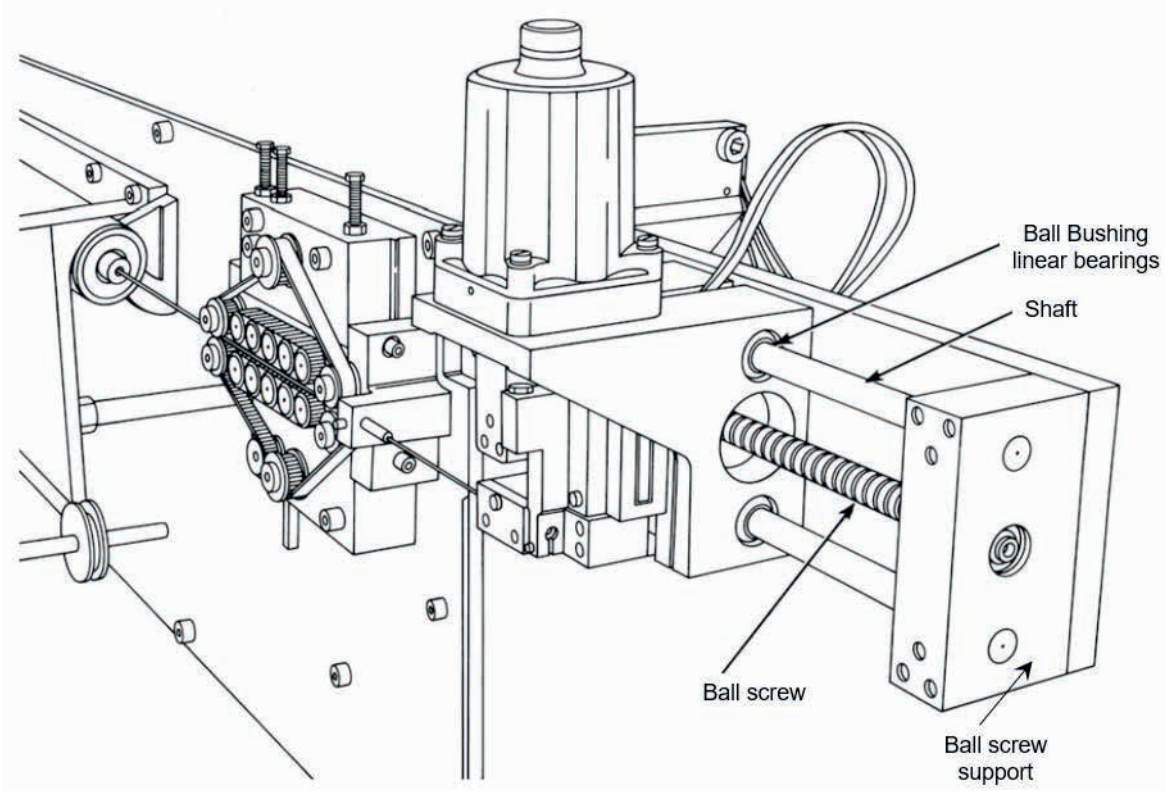

Figure 13 - Wire straightening/feeding machine (THOMSONLINEAR, 2023)

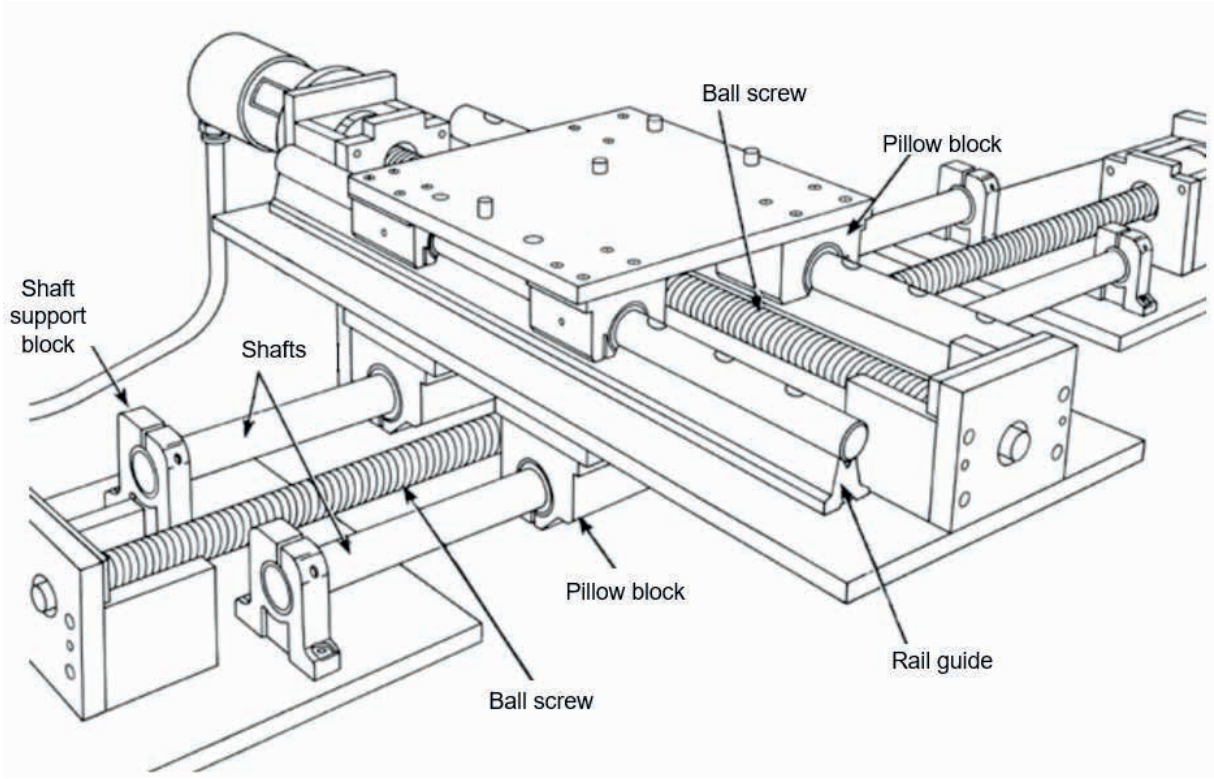

Figure 14 - Pick and place X-Y system (THOMSONLINEAR, 2023)

types include:

a) Bolts and Nuts: this is one of the most common types of detachable fastenings. A bolt is a threaded cylindrical fastener that passes through aligned holes in two or more components. It is secured by tightening a corresponding nut onto the threaded end of the bolt. Bolts and nuts provide a strong and reliable connection and can be easily tightened or loosened using tools such as wrenches or spanners.

b) Screws: are similar to bolts but typically have a pointed end and a threaded shaft along the entire length. They are usually used to fasten components by rotating them into pre-drilled holes or into threads on the mating component. Screws are commonly used in applications such as woodworking, construction, and electronics.

c) Rivets: are permanent fasteners used to join two or more components by deforming the end of the rivet to create a mechanical lock. They are commonly made of materials like steel, aluminum, or copper and are widely used in applications where a permanent, vibration-resistant connection is required, such as in aerospace and automotive industries.

d) Snap-fit connections: rely on the elasticity or flexibility of the components to create a secure attachment. They involve interlocking features, such as tabs and grooves or hooks and slots, which allow for easy assembly and disassembly without the need for additional fasteners. Snap-fit connections are commonly found in consumer products like plastic casings, electronic devices, and automotive interiors.

e) Clips and clamps: Clips and clamps are fasteners that provide a temporary or adjustable attachment. They often feature a spring mechanism or a clamping mechanism that allows for quick and easy installation and removal. They are commonly used for securing hoses, cables, and other flexible components in applications such as automotive, plumbing, and electrical installations.

These are just a few examples of detachable fastenings, and there are many other types available, each designed to suit specific applications and requirements. The choice of fastening method depends on factors such as the type of materials being joined, the required strength of the connection, ease of assembly and disassembly, and the specific needs of the application.

Pins are cylindrical or rod-shaped fasteners used to secure or connect two or more components together. They are versatile and widely used in various industries and applications. Pins are designed to provide a temporary or permanent connection, depending on the specific requirements of the application (RAEYMAEKERS, 2022).

There are different types of pins available, each with its own characteristics and applications. Here are some commonly used types of pins:

a) Straight pins: also known as dowel pins or alignment pins, are cylindrical pins with a uniform diameter along their entire length. They are used to align and position components accurately during assembly. Straight pins are typically press-fit into pre-drilled holes and provide precise location and stability. An example of dowel pin is shown in Figure 15.

Figure 15 - Wooden dowel pins (WIKIPEDIA, 2023a)

b) Clevis pins: also called hitch pins or quick-release pins, have a head at one end and a through-hole or cross-hole at the other end. They are commonly used for securing fastening components such as clevises, brackets, and linkages. Clevis pins can be easily inserted or removed without tools, making them convenient for quick assembly and disassembly. An example of clevis and clevis pins is shown in Figure 16.

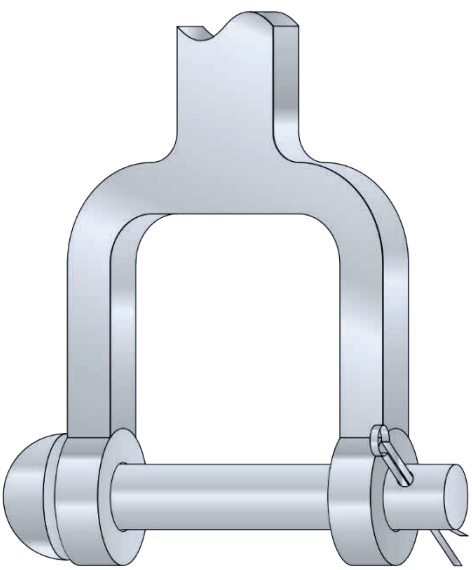

Figure 16 - A clevis and clevis pin, held in place by a split pin (WIKIPEDIA, 2023b)

c) Spring pins: also known as roll pins or coil pins, are hollow, cylindrical pins with a longitudinal slot along their length. They are designed to expand when inserted into a hole, creating a secure and tight fit. Spring pins are commonly used to prevent relative motion or rotation between two components and can withstand vibration and lateral forces. An example of spring pin is show in Figure 17.

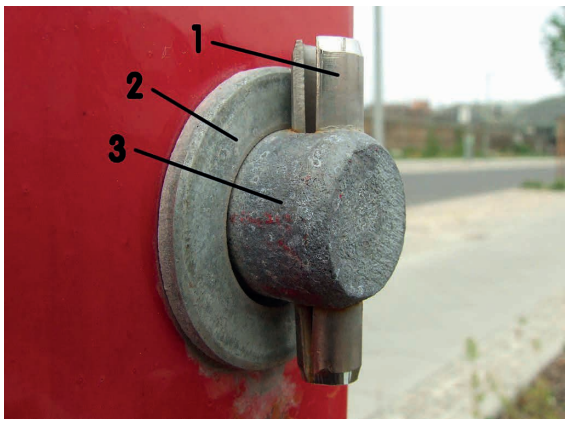

Figure 17 - Slotted spring pin (1) and washer (2) used to secure a shaft (3) (WIKIPEDIA, 2023c)

d) Taper pins: have a tapered shape with a larger diameter at one end and a smaller diameter at the other end. They are used for aligning and securing components with tapered holes. Taper pins provide a tight and reliable connection and are commonly used in applications such as machinery, automotive, and construction. An example of taper pin is shown in Figure 18.

e) Cotter pins: also known as split pins, cotter keys, bipartite pins or two-piece pins, are U-shaped pins with two tines that can be inserted into a hole or through a slot in a shaft or component. Once inserted, the tines are spread apart to prevent the pin from sliding out. Cotter

pins are often used to secure bolts, nuts, and other fasteners and provide a reliable locking mechanism. An example of split pin is shown in Figure 19.

These are just a few examples of pins used in various applications. Pins can be made from a variety of materials such as steel, stainless steel, brass, or aluminum, depending on the specific requirements of the application, including factors such as strength, corrosion resistance, and temperature resistance. The selection of the appropriate pin type depends on the specific application, load requirements, ease of assembly and disassembly, and other considerations related to the functionality and performance of the connected components (JADON & VERMA, 2014).

INTERFERENCE FIT

Interference fit refers to a type of assembly in which two mating parts are intentionally designed with tolerances that result in a tight, interference or press fit between them. In an interference fit, the diameter of the hole or bore in one component is intentionally smaller than the diameter of the shaft or pin that is meant to be inserted into it. Interference fits are also called press and shrink fits (METWALLI, 2021).

The purpose of an interference fit is to create a secure and rigid connection between the two mating parts. When the shaft or pin is pressed into the hole, the material of the components deforms slightly due to the interference between them. This deformation creates a frictional force and a mechanical interlock that helps prevent relative movement or separation between the parts.

Interference fits offer several advantages in various applications. They provide increased load-carrying capacity, improved resistance to vibration and shock, and enhanced precision and alignment. Interference fits can also help improve the overall strength and structural integrity of an assembly.

However, it's important to carefully consider the tolerances and dimensions when designing for an interference fit. The amount of interference should be calculated to ensure a proper fit without causing excessive stress, deformation, or damage to the mating parts. Thermal expansion and contraction should also be taken into account, as changes in temperature can affect the fit.

Interference fits are commonly used in various industries, including automotive, aerospace, machinery, and manufacturing, for applications such as bearing assemblies, press-fit connections, shafts, gears, and couplings.

It's worth noting that the specific requirements for an interference fit can vary depending on the application and the materials involved. Design considerations, such as the material properties, the intended load and stress conditions, and the desired level of interference, should be carefully evaluated to ensure the desired fit and performance of the assembly.

When two cylinders are joined together through a press fit or shrink fit, they form an assembly where the outer diameter of the inner cylinder is compressed due to the applied pressure, while the inner diameter of the outer cylinder experiences the same pressure from the inside. As a result, both cylinders undergo deformation at the interface, forming a shrink fit radius. In the context of this assembly, stress distributions can be observed both tangentially and radially. Figure 20 provides a visual representation of these stress patterns.

MATERIALS AND METHODS

Similar to other machine elements, the design of a machine base or frame requires careful consideration of the forces and moments exerted on these supporting structures by the mounted components during machine operation. Additionally, the weight

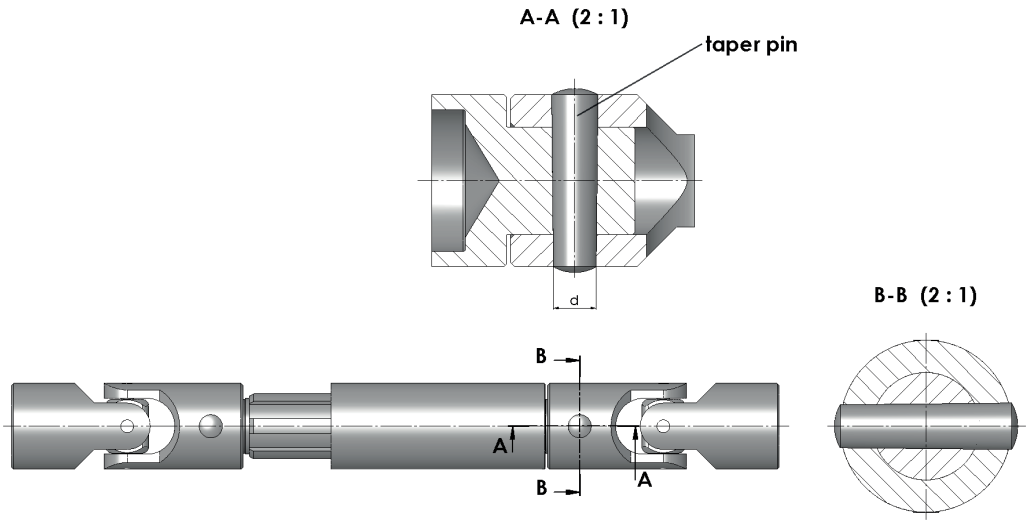

Figure 18 - An example of tapered pin used to lock two shafts together (WIKIPEDIA, 2023d)

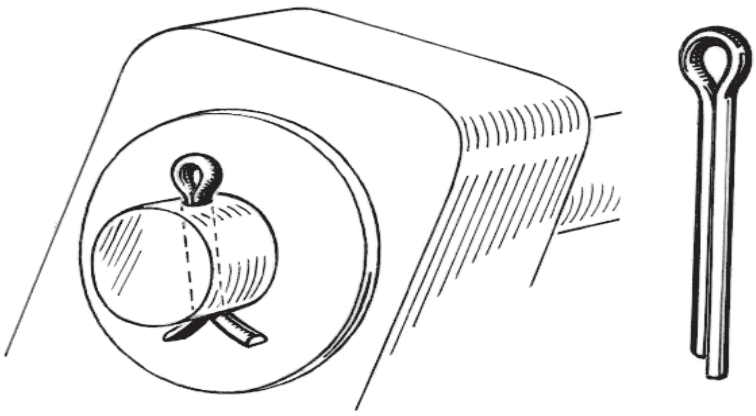

Figure 19 - A split pin (UK usage) / cotter pin (USA usage) holding a rod in place with a washer (WIKIPEDIA, 2023e)

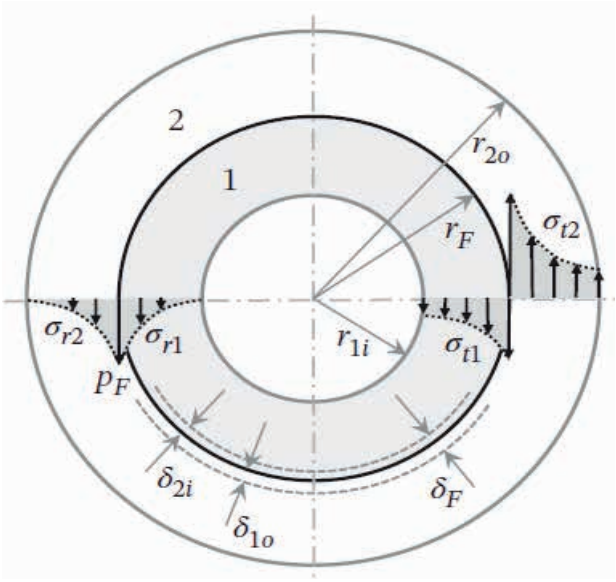

Figure 20 - Tangential and radial stress distributions are shown for two cylinders pressed together (METWALLI, 2021)

of the structural frame members must be taken into account in certain cases. Designing a frame involves evaluating potential failure modes, selecting suitable materials, and establishing an optimal structural geometry. An effective structural geometry should ensure the accuracy of spatial relationships between mounted components and provide reliable component support throughout the machine's design life, avoiding any instances of failure (COLLINS *et al*., 2009).

A crucial role of a base or frame is to serve as a robust structural support system for precisely positioning and assembling the various operational components. Figure 21 showcases different types of frames, such as baseplates, open-truss frames, shell structures, C-frames, O-frames, housings, and unique combinations thereof. These frames offer distinct design configurations tailored to specific applications and requirements, ensuring the secure mounting and integration of components.

Shaft support blocks serve as a suitable choice for providing end or intermittent support in applications where the loads are relatively light and shaft deflection is not a critical factor. Unlike shaft support rails, these blocks do not allow for the longitudinal movement of open-type ball bushing bearings. By utilizing shaft support blocks, shafts can be securely clamped, eliminating the necessity for bolts to maintain shaft position. For high precision applications, it is recommended to employ shimming techniques to mitigate the impact of surface variations in the base or manufacturing tolerances between the supports (THOMSONLINEAR, 2023). There are several configurations of shaft support blocks. Some of them are shown in Figure 22.

In situations where surface conditions or spans do not permit continuous support, the use of end supports becomes necessary for the installation of round shafting. Support blocks are employed to bridge gaps ranging from 4 to 12 times the diameter of the shaft. However, it is important to consider the potential for deflection when dealing with such extended lengths. Unlike square rail systems, round rail configurations are more forgiving when it comes to accommodating deflection and misalignment, especially when combined with suitable bearings. By opting for self-aligning bearings that offer a tolerance of up to ±1/2 degree of misalignment, smooth and unhindered motion can be maintained, even in cases where standard bearing designs would result in binding. Support blocks are readily available for end or intermittent mounting, and they can also be obtained in a flanged form for perpendicular mounting applications. Examples of support blocks applications are shown in Figure 23.

In this article, a shaft supporting block was designed for a specialized mechanical application. Due to confidentiality reasons, the specific details of the equipment and company using it cannot be disclosed. However, for the sake of illustrating the design process, the application forces will be mentioned in this article without providing specific information about the equipment. This approach ensures the preservation of confidentiality while allowing us to discuss the considerations and design principles involved in developing the shaft supporting block for the given application. The shaft supporting block mounting is shown in Figure 24.

The Computer Aided Design (CAD) files of this shaft is available at: https://grabcad.com/library/representacao-didatica-de-um-mancal-1.

In technical drawing an exploded view is a graphical representation that shows the individual components of an assembly separated from each other, often with reference lines or arrows indicating the intended assembly sequence. It provides a

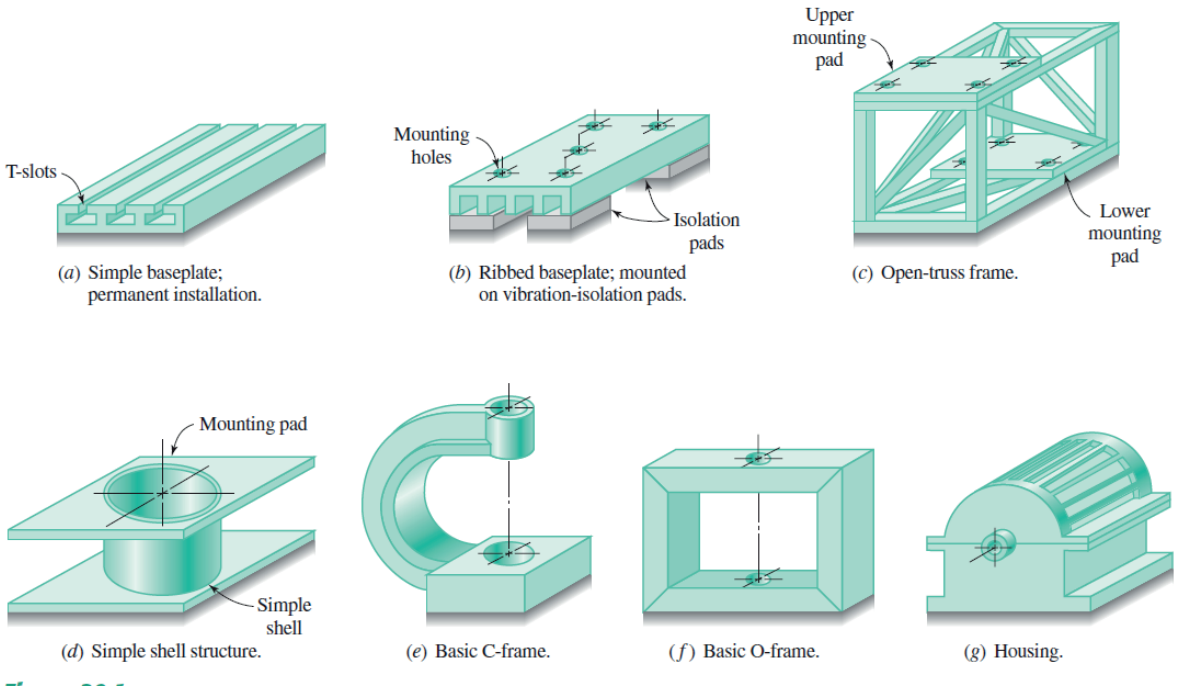

Figure 21 - Illustration of several common types of machine frames (COLLINS et al., 2009)

Figure 22 - Thomson shaft support blocks (THOMSONLINEAR, 2023)

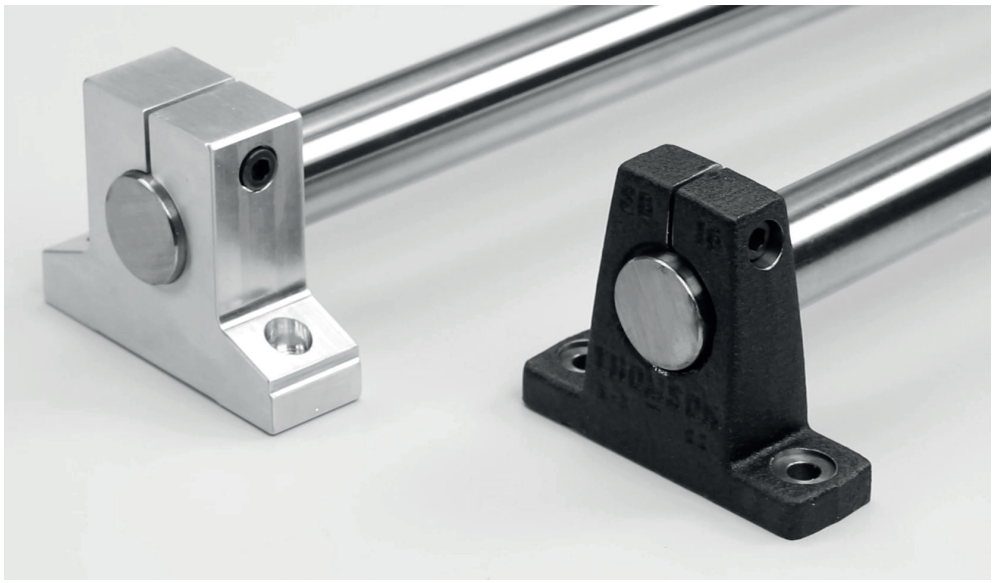

Figure 23 - Support blocks are utilized to secure the shaft either at its ends or intermittently, ensuring its stable and fixed position (THOMSONLINEAR, 2023)

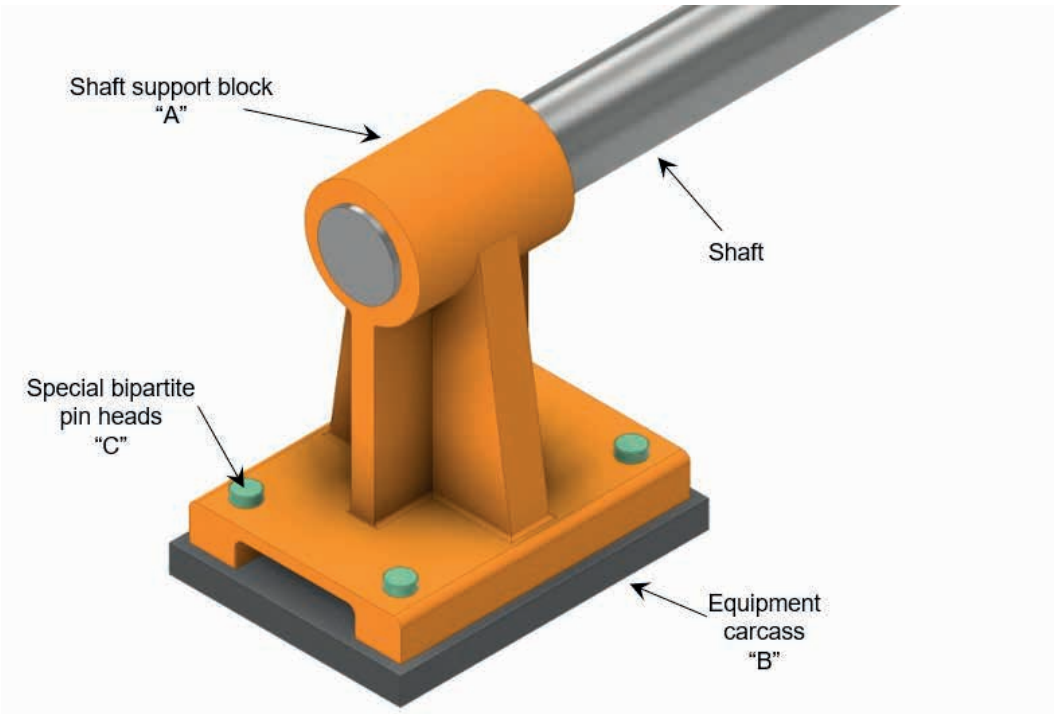

Figure 24 - Shaft support block mounting scheme

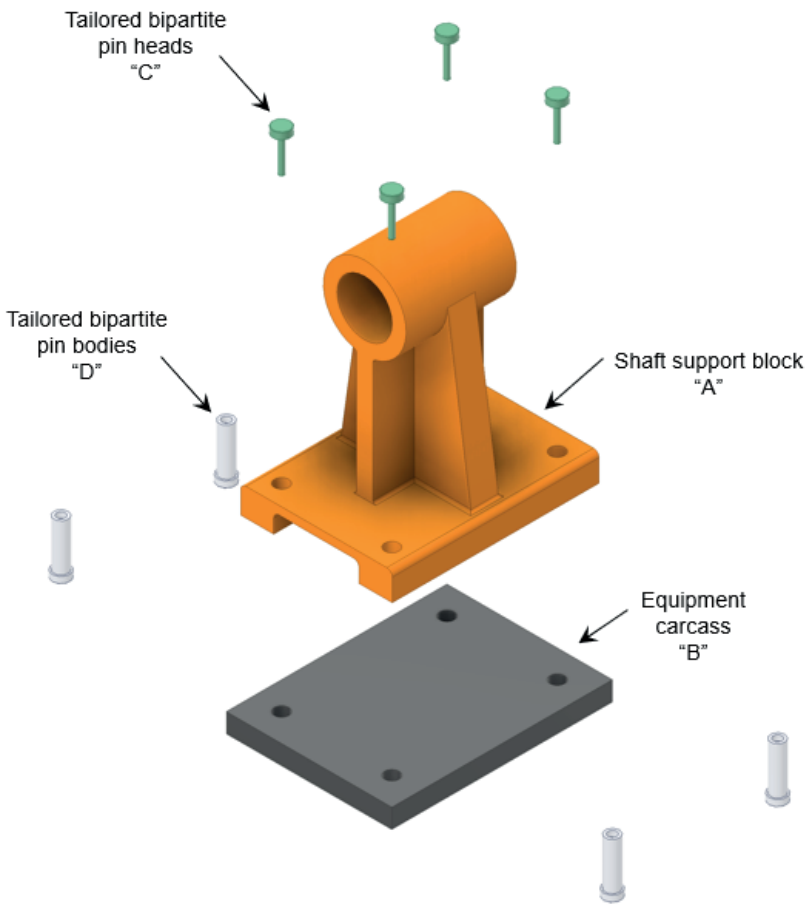

Figure 25 - Shaft support block mounting scheme exploded view

clear understanding of how the different parts fit together and is commonly used in technical documentation, manuals, and engineering designs.

In the exploded view shown in Figure 25, the shaft support block is referred to as "A" and the equipment carcass as "B". On the other hand, tailored bipartite pins heads, shown in green, are referred to as "C". The tailored bipartite pins bodies, that are not depicted in the previous figure, are referred to as "D".

The tailored bipartite pin parts featured in the shaft support block mounting scheme are illustrated in Figure 26.

The cross-sectional and isometric views of the tailored bipartite pin assembly, offering readers detailed insights into its design and configuration, are shown in Figure 27.

There are a few reasons to justify the application of the tailored bipartite pins, or customized dual-fit fasteners, instead one of the traditional pins. Some of them are listed below:

a) Enhanced alignment: the configuration of the mating parts provides improved alignment between the two components being fastened. The mating surfaces ensure precise positioning, reducing misalignment and enhancing overall accuracy in the assembly (SPECK, 2015).

b) Increased stability: the mating parts offer enhanced stability and resistance to loosening or disengagement. The design creates a secure and robust connection, minimizing the risk of unwanted movement or separation of the components (TAMBOLI, 2016).

c) Improved load distribution: the mating parts help distribute the applied loads more evenly across the joint interface. The contact area between the mating surfaces allows for a larger load-bearing surface, reducing localized stress concentrations and improving overall load-carrying capacity (CHILDS, 2021).

d) Enhanced rigidity: the mating parts provide increased rigidity and stiffness to the assembly. The interlocking design enhances the structural integrity, minimizing flexing or bending under applied loads and maintaining the desired mechanical stability (STERKENBURG & WANG, 2021).

e) Easy assembly and disassembly: the mating parts allow for convenient assembly and disassembly of the components. The fitting of the parts together facilitates quick and efficient installation, while also providing ease of disassembly for maintenance, repairs, or component replacement (PARMLEY, 2000).

RESULTS AND DISCUSSIONS

In this study, we investigated the interference fit requirements for customized dual-fit fastening pins. The linear guide rail mounting dimensions are presented in millimeters in Figure 28.

The force F is exerted by the shaft onto the shaft support block during equipment operation. Surface B is where the shaft support block is attached, meaning that the tailored bipartite pin components "C" and "D" detachably fasten surfaces "A" and "B". All dimensions are displayed in millimeters and the part letters (A, B, C, D) are displayed in bold.

The assembly in the figure shows a cast iron shaft support block A fixed to a bronze structure B by four equidistant customized dua-fit steel pins. Piece A is subjected to a vertical force F=60 kN applied along the axis of symmetry of parts A and B. The customized dual-fit pins are manufactured in two parts (C and D) and assembled by a longitudinal press

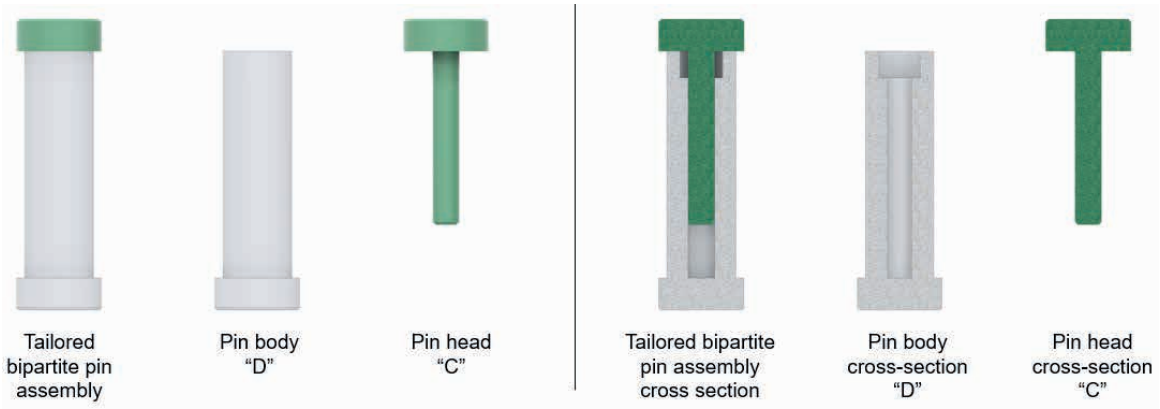

Figure 26 - Tailored bipartite pins configuration

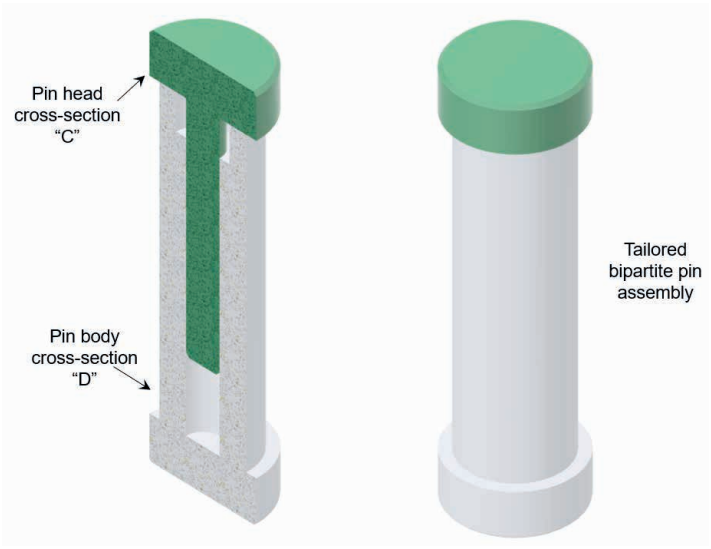

Figure 27 - Tailored bipartite pins assembly cross-sectional and isometric views

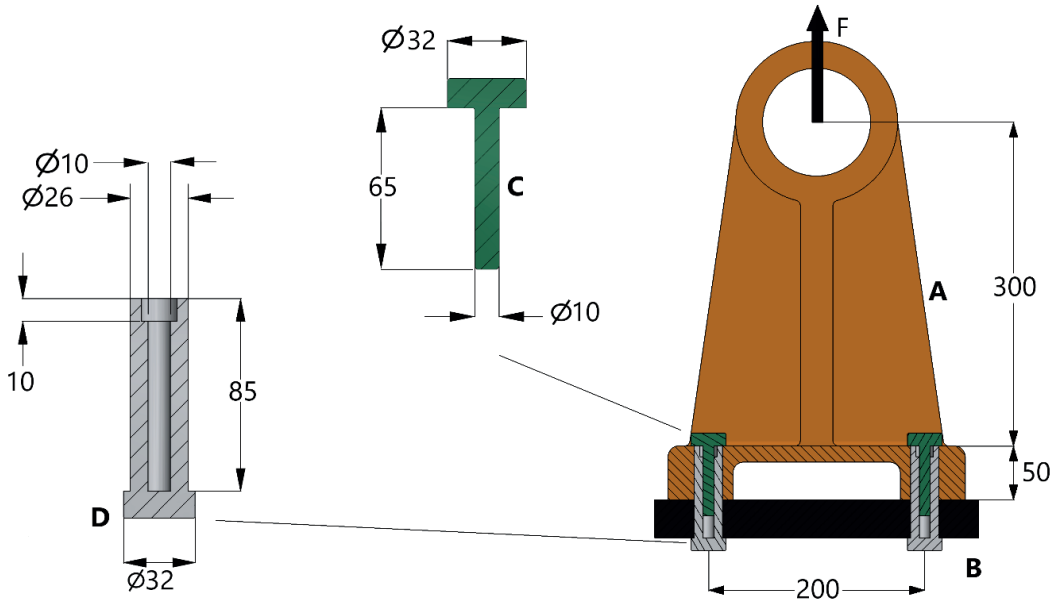

Figure 28 - Technical drawings of shaft support block and tailored bipartite pins

fit without lubrication. The interference does not cause significant compression between parts A and B.

During the pin manufacturing process, the average surface roughness of both parts is 1.5 μm. Part C was manufactured with IT7 specification, while part D has an IT8 specification. The design of these two parts was based on the assumption of a basic hole. The dynamic friction coefficient between the components of the pin is 0.30.

Consider the following material properties:

a) Steel used for both parts of the pins: axial modulus of elasticity (E) of 210 GPa; Poisson's ratio (v) of 0.3; yield strength (σ_e) of 1125 MPa; ultimate tensile strength (σ_r) of 1375 MPa.

b) Cast iron used for the fabrication of part A: E=100 GPa; v=0.25; σ_e=135 MPa; σ_r=178 MPa.

c) Bronze used for the fabrication of part B: E=109 GPa; v=0.32; σ_e = 56 MPa; σ_r=67 MPa.

The objective was to determine the precise interference fit for the customized dual-fit pins, ensuring they could withstand the applied force effectively.

According to Bhandari (2010), complex components that pose challenges for conventional machining processes can be effectively produced through the casting method utilizing sand molds. The versatility of casting allows for the use of a wide range of metals, with cast iron, aluminum alloys, and brass being commonly employed for sand cast parts. These castings exhibit surfaces with irregularities and a grainy texture, necessitating machining when the part interacts with other moving components or structures. Cast components offer excellent stability, rigidity, and strength compared to their machined or forged counterparts.

Examples of typical cast components include machine tool beds and structures, cylinder blocks for internal combustion engines, pump bodies, and gearbox housings. It should be noted that the strength of a cast iron component can be more adversely affected by poor shaping than the actual material composition. To ensure a successful design, collaboration with both the foundry professional and the patternmaker is crucial, as they possess invaluable expertise in casting processes. Balanced sections with equal areas subjected to tension and compression are not recommended for cast iron components.

Optimal positioning of castings involves exposing them predominantly to compressive rather than tensile stresses. In cases where tensile stresses are unavoidable, the implementation of a clamping device, such as a tie rod or a bearing cap, is advisable (BHANDARI, 2010). A typical application of casting under different stresses is shown in Figure 29.

The nominal dimension of the parts is the external diameter of the shaft (Ø10 mm) and the internal diameter of the outer piece (Æ10 mm). We know that the basic hole assumption should be considered. Therefore, we know that the hole has its tolerance in the H field. At the same time, we also know the International Tolerances (IT) for each part: hole IT8 and shaft IT7. In other words, almost all information about the fit is known, except for the letter that identifies the allowance of the shaft. Therefore, the fit specification is: Ø10H8_7. When consulting the adjustment tables for HOLES and shafts in NBR 6158:1995, we find that: $A_{máx}$=22 μm; $A_{mín}$=0 μm.

The assembly of these parts is done through longitudinal force fit. Therefore, there is a loss of interference during the assembly process, which needs to be calculated using the specified empirical relationship: $\Delta I=1{,}2(Ra_{CUBO}+Ra_{eixo})$. In this case, we know that the average surface roughness of both parts of the pin is 1.5 μm.

Therefore ΔI=1.2(1.5+1.5)=3.6 mm.

Interpreting the system's operation is crucial for performing calculations in a coherent manner. An interference fit has the theoretical ability to transmit both torque (T) and axial force (F_a) simultaneously. The key is to determine the magnitudes of the torque and axial force to ensure transmission without slippage and in a safe manner. In the application described in the statement, there is no torque transmission; only the requirement for the applied force to be supported without the separation of surfaces A and B. Therefore, the external force acting on the system introduces an axial force to the 4 pins used for fastening. Consequently, each pin will need to withstand 1/4 of the external force. In our application, the external forces are: F_a=60/4=15 kN and T=0.

The dynamic friction coefficient between the components of the pin is 0.30. Therefore, μ_D=0.30. Using the known empirical relationship: $\mu_D=0.5\cdot\mu_D \therefore 0.30=0.5\cdot\mu \therefore \mu=0.60$.

To finally apply the slippage criterion and calculate the minimum pressure for the specified fit to transmit the loads, it is important to determine the effective contact length where interference occurs. Please note that when assembling the upper part of the pin (shaft) into the lower part of the pin (HUB), the effective contact length (L) is obtained by performing the following algebraic operation: L=65-10=55 mm. The length of the shaft is 65 mm, but due to the geometry of the HUB, which has a recess of 10 mm, only 55 mm of the two parts remain in contact. Therefore, we can finally apply the slippage criterion between components joined by interference.

$$\pi \cdot \mu \cdot d \cdot L \cdot p_{min} \geq \sqrt{F_a^2 + \left(\frac{2 \cdot T}{d}\right)^2} \therefore \pi \cdot$$

$$0.60 \cdot 10 \cdot 55 \cdot p_{min} \geq \sqrt{15000^2 + \left(\frac{2 \cdot 0}{10}\right)^2}$$

$$p_{min} \geq 14.47\ MPa$$

As the dimensions are known, the internal (shaft) and external (HUB) parts need to have their geometric factors determined (Q). The shaft is solid, therefore Q_i=0. The HUB has its internal and external diameters defined as 10 mm and 26 mm, respectively.

$$Q_i = \frac{d_i}{d_e} = \frac{0}{10} = 0\ ;\ Q_e = \frac{D_i}{D_e} = \frac{10}{26} = 0.38$$

We know that both parts of the pin are made of the same material, which is steel. Therefore, it is possible to determine the elastic factors (K) of these two parts.

$$K_i = \frac{1}{E_i} \cdot \left(\frac{1 + Q_i^2}{1 - Q_i^2} - \nu_i\right) = \frac{1}{210000} \cdot \left(\frac{1 + 0^2}{1 - 0^2} - 0.30\right) =$$

$$3.333 \cdot 10^{-6} \frac{mm^2}{N} = 3.333 \cdot 10^{-6} MPa^{-1}$$

$$K_e = \frac{1}{E_e} \cdot \left(\frac{1 + Q_e^2}{1 - Q_e^2} + \nu_e\right) = \frac{1}{210000} \cdot \left(\frac{1 + 0.38^2}{1 - 0.38} + 0{,}30\right) =$$

$$7.844 \cdot 10^{-6} \frac{mm^2}{N} = 7.844 \cdot 10^{-6} MPa^{-1}$$

Therefore, it is possible to calculate, based on the relationship between pressure and post-assembly interference, the minimum interference required to prevent slippage between the parts of the pin and the subsequent separation of parts A and B.

$$p_{min} = \frac{Z_{min} \cdot 10^{-3}}{(K_i + K_e) \cdot d_{eixo}} \therefore 14.47 =$$

$$\frac{Z_{min} \cdot 10^{-3}}{(3.333 \cdot 10^{-6} + 7.844 \cdot 10^{-6}) \cdot 10}$$

$$Z_{min} = 0.001617\ mm = 1.62\ \mu m$$

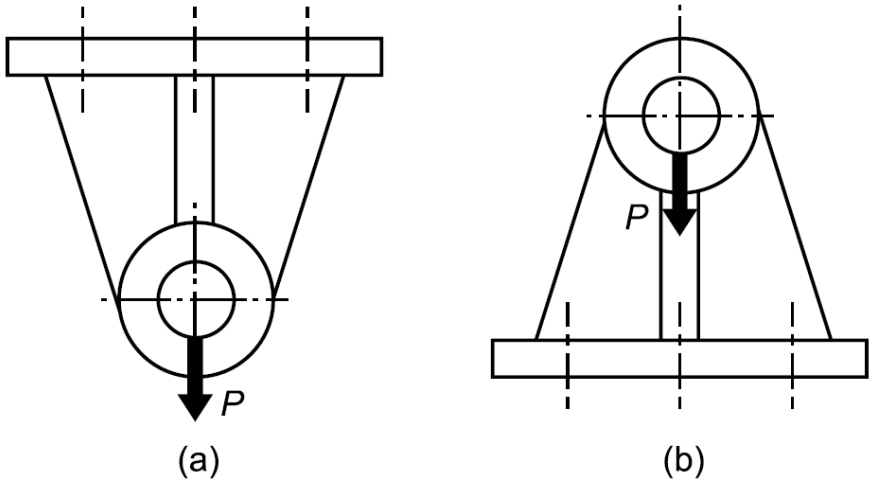

Figure 29 - Castings subjected to (a) tensile stresses and (b) compressive stresses (BHANDARI, 2010)

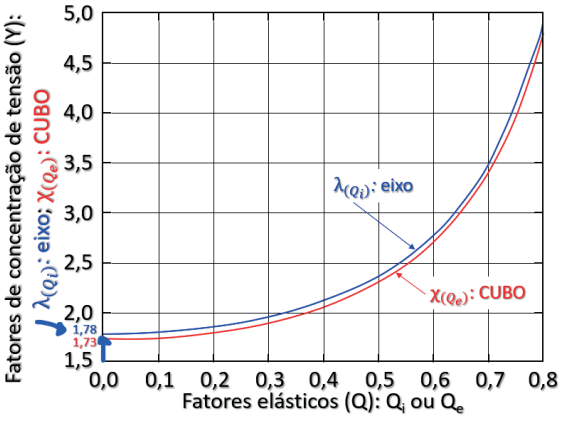

Shaft => $\lambda_{(Qi=0)} = 1.78$

$$p_{max} \cdot \lambda_{(Q_i)} \leq \frac{\sigma_{e_{eixo}}}{n_{mec_{eixo}}}$$

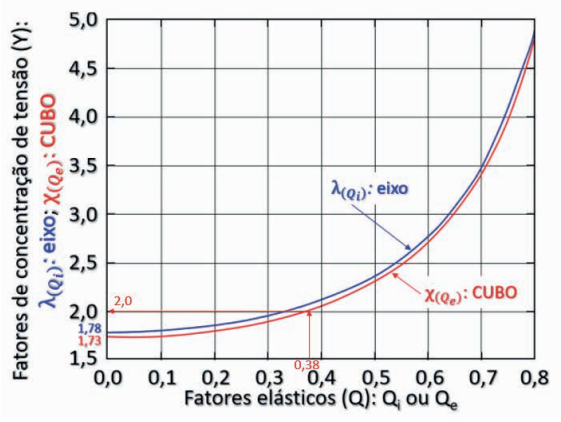

HUB => $X_{(Qe=0.769)}$=2.00

$$p_{max} \cdot \chi_{(Q_e)} \leq \frac{\sigma_{e_{CUBO}}}{n_{mec_{CUBO}}}$$

Using the concepts of post-assembly interference (Z), we know that:

$$Z_{min} = I_{min} - \Delta I \therefore 1.62 = I_{min} - 3.6 \therefore I_{min} = 1.62 + 3.6 = 5.22\ \mu m$$

Using the concepts of pre-assembly interference (I), we know that:

$$I_{min} = a_{min} - A_{max} \therefore 5.22 = a_{min} - 22 \therefore a_{min} = 27.22\ \mu m$$

Therefore, we can select the fit by fixing the nominal diameter line of 10 mm in the dimensional tables and analyzing the columns for IT7 shafts. We need to find the first minimum shaft allowance that is greater than or equal to 27.22 μm. This search returns a minimum shaft allowance of 34 μm, which corresponds to the tolerance class x7. Therefore, the fit specification is: Ø10H8u7 ($A_{máx}$=22 mm; $A_{mín}$=0 mm; $a_{máx}$=43 mm; $A_{mín}$=28 mm).

For the following calculations, we should use the values of the relevant allowances for the selected specification. Therefore:

$$Z_{max} = I_{max} - \Delta I = a_{max} - A_{min} - \Delta I = 43 - 0 - 3.6 = 39.40\ \mu m$$

In this way, it is possible to determine the maximum pressure between the parts.

$$p_{max} = \frac{Z_{max} \cdot 10^{-3}}{(K_i + K_e) \cdot d_{eixo}} = \frac{39.40 \cdot 10^{-3}}{(3.333 \cdot 10^{-6} + 7.844 \cdot 10^{-6}) \cdot 10} = 352.50\ MPa$$

The stress concentration factor (n_{mec}) is a function of the geometry of each part, depending on the geometric factor of each individual piece. It is necessary to consult the stress concentration factor for each part using the graphs provided in reference books. Since the geometric factors are known, it is straightforward to determine the stress concentration factors.

It is observed that both stress concentration factors are greater than 1. This indicates that the parts would not fail in the case of assembling the larger shaft with the smaller hole (where maximum interference occurs between the parts, resulting in maximum pressure between the contact surfaces).

CONCLUSIONS

In this study, we investigated the interference fit requirements for customized bipartite fastening pins in a linear guide rail mounting application. Through our calculations and analysis, we were able to optimize the frictional force in the shaft support mount attachment using bipartite fastening pins. Our results demonstrate that the interference fit between the two parts of the bipartite pin significantly affects the frictional force required to hold the shaft support mount attached to the surface.

We found that the diameter, material, and surface roughness of the bipartite fastening pins all play a role in the required interference fit for optimal frictional force. By considering these factors, engineers and designers can better select and design bipartite fastening pins for similar applications.

Overall, our research provides important insights into the use of bipartite fastening pins in linear guide rail mounting applications and can inform the development of more efficient and effective mounting systems. Our calculations and analysis demonstrate the feasibility of using bipartite fastening pins to attach shaft support mounts to surfaces, and we believe that our findings can be of great value to researchers and professionals in the field of mechanical engineering.

In summary, the results of our study show that bipartite fastening pins can be a reliable and effective method for attaching shaft support mounts to surfaces in linear guide rail mounting applications, provided that the necessary interference fit requirements are met. We hope that our research can

inspire further investigation into the use of bipartite fastening pins and contribute to the development of more innovative and efficient mounting systems in the future.

ACKNOWLEDGEMENTS

The authors would like to express their sincere gratitude to their families for their unwavering support throughout the course of this research. We would also like to acknowledge the academics institutions Fatec Mauá and Centro Universitário FEI for providing us with the necessary resources and infrastructure to carry out this work.

REFERENCES

[1] ABNT. NBR 6158. **Sistema de tolerâncias e ajustes**. 1995.

[2] BHANDARI, V. B.. **Design of Machine Elements**. 3. ed. McGraw-Hill, 2010. 958 p. (ISBN-13: 978-0070681798).

[3] CHANG, Jyh-Cheng; HUNG, Jui-Pin. Analytical and Finite Element Modeling of the Dynamic Characteristics of a Linear Feeding Stage with Different Arrangements of Rolling Guides. **Mathematical Problems In Engineering**, [S.L.], v. 2014, p. 1-11, 2014. Hindawi Limited. http://dx.doi.org/10.1155/2014/454156.

[4] CHILDS, P.R.N.. Fastening and Power Screws. **Mechanical Design**, [S.L.], p. 371-412, 2021. Elsevier. http://dx.doi.org/10.1016/b978-0-12-821102-1.00010-x.

[5] COLLINS, Danielle. **Don't ignore these three things when mounting linear guides**. 2015. Available at: https://www.linearmotiontips.com/dont-ignore-these-three-things-when-mounting-linear-guides/. Access in: 16 May 2023.

[6] COLLINS, Jack A.; BUSBY, Henry R.; STAAB, George H.. **Mechanical Design of Machine Elements and Machines**: failure prevention perspective. 2. ed. Wiley, 2009. 912 p. (ISBN: 978-0-470-41303-6). https://www.wiley.com/en-us/Mechanical+Design+of+Machine+E lements+and+Machines%3A+A+ Failure+Prevention+ Perspective%2C+2nd+Edition-p-9780470413036.

[7] GROSS, Dietmar; HAUGER, Werner; SCHRÖDER Jörg; WALL, Wolfgang A.; RAJAPAKSE, Nimal**. Engineering Mechanics 1**. 2. ed. Springer, 2013. 306 p. (ISBN 978-3-642-30318-0). DOI 10.1007/ 978-3-642-30319-7. https://link.springer.com/book/10.1007/978-3-642-30319-7

[8] JADON, V K.; VERMA, Suresh. **Analysis and Design of Machine Elements**. 2. ed. New Delhi - 110002, Delhi, India: I.K International Pvt. Ltd., 2014. 1000 p. (ISBN: 9789384588106). Https://www.ikbooks.com/books/book/engineering-computer-science/mechanical-production-industrial-engineering/analysis-design-machine-elements/9789384588106/.

[9] JIANG, Wei. **Analysis and Design of Machine Elements**. Wiley, 2019. 528 p. (ISBN: 978-1-119-27607-4). https://www.wiley.com/en-us/Analysis+and+Design+of+Machine+Elements-p-9781119276074.

[10] KRAMPERT, David; UNSLEBER, Sebastian; REINDL, Leonhard. Localized Surface Strain Measurement for Load Detection Using Diamond like Carbon Coating on a Linear Guide. **2021 IEEE International Instrumentation And Measurement Technology Conference (I2Mtc)**, [S.L.], v. 5, n. 8, p. 327-345, 17 May. 2021a. IEEE. http://dx.doi.org/10.1109/i2mtc50364.2021.9459827.

[11] KRAMPERT, David; ZIEGLER, Mario; UNSLEBER, Sebastian; REINDL, Leonhard; RUPITSCH, Stefan J.. On the stiffness hysteresis of profiled rail guides. **Tribology International**, [S.L.], v. 160, p. 107019, Aug. 2021b. Elsevier BV. http://dx.doi.org/10.1016/j.triboint.2021.107019.

[12] LI, Xinxin; LI, Zhi-Min; JIN, Sun; ZHANG, Jichang; DING, Siyi; NIU, Zhihua. A Novel Error Equivalence Model on the Kinematic Error of the Linear Axis of High-End Machine Tool. **He International Journal Of Advanced Manufacturing Technology**, [S.L.], v. 5, n. 8, p. 327-345, 23 Mar. 2021. Research Square Platform LLC. http://dx.doi.org/10.21203/rs.3.rs-328470/v1.

[13] LIU, Zhendong; XU, Mengtao; ZHANG, Hongzhuang; LI, Changyou; YAO, Guo; MIAO, Huihui; WANG, Chenyu; ZHANG, Yimin. Modeling and Analyzing of Nonlinear Dynamics for Linear Guide Slide Platform Considering Assembly Error. **Nonlinear Dynamics**, [S.L.], v. 5, n. 8, p. 327-345, 23 Aug. 2021a. Research Square Platform LLC. http://dx.doi.org/10.21203/rs.3.rs-817365/v1.

[14] LIU, Meng; XIA, Yuan; LU, Hong; ZHANG, Yongquan; ZANG, Yue; LI, Le. A Straightening Control System for the Linear Guide Rail. **2021 IEEE 5Th Advanced Information Technology, Electronic And Automation Control Conference (Iaeac)**, [S.L.], v. 5, n. 8, p. 327-345, 12 Mar. 2021b. IEEE. http://dx.doi.org/10.1109/iaeac50856.2021.9390730.

[15] LIU, Tinghao; HAO, Guangbo. Design of a Cylindrical Compliant Linear Guide with Decoupling Parallelogram Mechanisms. **Micromachines**, [S.L.], v. 13, n. 8, p. 1275, 8 Aug. 2022. MDPI AG. http://dx.doi.org/10.3390/mi13081275.

[16] METWALLI, Sayed M.. **Machine Design with CAD and Optimization**. Wiley, 2021. 1008 p. (ISBN: 978-1-119-15664-2). https://www.wiley.com/en-us/Machine+Design+with+CAD+and+Optimization-p-9781119156642.

[17] NGUYEN, Van-Khien; PHAM, Huy-Tuan; PHAM, Huy-Hoang; DANG, Quang-Khoa. Optimization design of a compliant linear guide for high-precision feed drive mechanisms. **Mechanism And Machine Theory**, [S.L.], v. 165, p. 104442, Nov. 2021. Elsevier BV. http://dx.doi.org/10.1016/j.mechmachtheory.2021.104442.

[18] PARMLEY, Robert O.. **Illustrated Sourcebook of Mechanical Components**. McGraw-Hill Professional, 2000. (ISBN 13: 9780070486171). Https://www.mhprofessional.com/illustrated-sourcebook-of-mechanical-components-9780070486171-usa.

[19] RAEYMAEKERS, Bart. **Design of Mechanical Elements**: a concise introduction to mechanical design considerations and calculations. Wiley, 2022. 256 p. (ISBN: 978-1-119-84996-4). https://www.wiley.com/en-us/Design+of+Mechanical+Elements%3A+A+Concise+Introduction+to+Mechanical+Design+Considerations+and+Calculations-p-9781119849964.

[20] ROMMERS, J.; NAVES, M.; BROUWER, D. M.; HERDER, J. L.. A Flexure-Based Linear Guide With Torsion Reinforcement Structures. **Journal Of Mechanisms And Robotics**, [S.L.], v. 14, n. 3, p. 1-9, Jun. 2022. ASME International. http://dx.doi.org/10.1115/1.4052971.

[21] SA'DIYAH, Halimatus; DARWITO, Purwadi Agus; TAVIO, Tavio; RADITYA, Murry. Design and Modelling of Ballscrew Linear Guide Actuator for Earthquake Shaking Table (EST) Based on Neural Network. **Iptek Journal Of Proceedings Series**, [S.L.], n. 6, p. 372, 15 Oct. 2021. Lembaga Penelitian dan Pengabdian kepada Masyarakat ITS. http://dx.doi.org/10.12962/j23546026.y2020i6.11125.

[22] SHAUKHAROVA, Azhar; LIANG, Yi; FENG, Hutian; XU, Bin. Study of Stiffness of Linear Guide Pairs by Experiment and FEA. **World Journal Of Engineering And Technology**, [S.L.], v. 04, n. 03, p. 115-128, 2016. Scientific Research Publishing, Inc.. http://dx.doi.org/10.4236/wjet.2016.43d015.

[23] SHIH, Wei-Cheng; FURQANUDDIN, Furqan; LEE, Po-Lin; HUNG, Jui-Pin. Monitoring of Preload Variation of Linear Guide Positioning Stage Using Artificial Neural Network. **Applied Sciences**, [S.L.], v. 11, n. 17, p. 7902, 27 Aug. 2021. MDPI AG. http://dx.doi.org/10.3390/app11177902.

[24] SKAKOON, James G.. **The Elements of Mechanical Design**. New York: ASME, 2008. 104 p. (ISBN: 9780791802670). Https://www.asme.org/publications-submissions/books/find-book/elements-mechanical-design/print-book.

[25] SONG, Xianchun; CHEN, Hongjian; JIANG, Hongkui; XU, Xiangrong; LI, Yanfeng; ZHANG, Yingshang. Improved design of roller linear guide for heavy load based on finite element method and measurement. **Advances In Mechanical Engineering**, [S.L.], v. 10, n. 9, p. 168781401880015, Sep. 2018. SAGE Publications. http://dx.doi.org/10.1177/1687814018800158.

[26] SPECK, James A.. **Mechanical Fastening, Joining, and Assembly**. 2. ed. Oxfordshire, England, Uk: Routledge, 2015. 384 p. (ISBN 9781138748408). https://www.routledge.com/Mechanical-Fastening-Joining-and-Assembly/Speck/p/book/9781138748408#.

[27] STERKENBURG, Ron; WANG, Peng Hao. **Standard Aircraft Handbook for Mechanics and Technicians, Eighth Edition**. 8. ed. McGraw-Hill Professional, 2021. (ISBN 13: 9781260468922). Https://www.mhprofessional.com/standard-aircraft-handbook-for-mechanics-and-technicians-eighth-edition-9781260468922-usa.

[28] SUN, Wei; KONG, Xiangxi; WANG, Bo. Precise finite element modeling and analysis of dynamics of linear rolling guideway on supporting direction. **Journal Of Vibroengineering**, v. 15, n. 3, p. 1330-1340, September. 2013. Https://www.extrica.com/article/14631.

[29] TAMBOLI, Akbar R.. **Handbook of Structural Steel Connection Design and Details**. 3. ed. McGraw-Hill Professional, 2016. (ISBN 13: 9781259585517). 9781259585517 https://www.mhprofessional.com/handbook-of-structural-steel-connection-design-and-details-third-edition-9781259585517-usa .

[30] THOMSONLINEAR. **RoundRail Linear Guides and Components**. 2023. Available at: https://www.thomsonlinear.com/downloads/bearings_guides/RoundRail_LinearGuides_Components_cten.pdf. Access in: 16 May 2023.

[31] WEI, Jiayong; LI, Cancan; MA, Yali. Finite element model for static characteristic analysis of rolling linear guide. **Proceedings Of The Institution Of Mechanical Engineers, Part C**: Journal of Mechanical Engineering Science, [S.L.], v. 236, n. 3, p. 1721-1732, 19 Jul. 2021. SAGE Publications. http://dx.doi.org/10.1177/09544062211021443.

[32] WIKIPEDIA. **Dowel**. 2023a. Available at: https://en.wikipedia.org/wiki/Dowel. Access in: 16 May 2023.

[33] WIKIPEDIA. **Clevis fastener**. 2023b. Available at: https://en.wikipedia.org/wiki/Clevis_fastener. Access in: 16 May 2023.

[34] WIKIPEDIA. **Spring pin**. 2023c. Available at: https://en.wikipedia.org/wiki/Spring_pin. Access in: 16 May 2023.

[35] WIKIPEDIA. **Spring pin**. 2023c. Available at: https://en.wikipedia.org/wiki/Spring_pin. Access in: 16 May 2023.

[36] WIKIPEDIA. **Taper pin**. 2023d. Available at: https://en.wikipedia.org/wiki/Taper_pin. Access in: 16 May 2023.

[37] WIKIPEDIA. **Split pin**. 2023e. Available at: https://en.wikipedia.org/wiki/Split_pin. Access in: 16 May 2023.

APPENDIX A

The main author of this article is a university professor at an Engineering college with extensive experience in the subject of Machine Elements. This discipline includes the specification of mechanical assemblies between cubes and shafts. One of the well-known techniques is interference fit, which is widely covered in reference books such as Shigley, Norton, Juvinall, Collins, among others. To facilitate his lectures, the professor has created a form that contains the most common mathematical expressions. All mathematical expressions are found in reference books. However, each book uses different terminology to describe each variable. The following figure presents the variables, their units, and the mathematical relationships.

Uniões por interferência

Diâmetros [mm]: CUBO => *D*: nominal; D_e: externo; D_i: interno; eixo=> *d*: nominal; d_e: externo; d_i: interno.

p: pressão entre as peças (CUBO/eixo) em decorrência da interferência entre elas [MPa]. T: torque [Nmm]; força axial F_a [N]. Índices usados nas fórmulas => i: peça interna; e: peça externa. Notação dos afastamentos => CUBO: LETRA MAIÚSCULA; eixo: letra minúscula.

Afastamentos [µm] => eixo: a_{min} ; a_{max} FURO: A_{min} ; A_{max}.

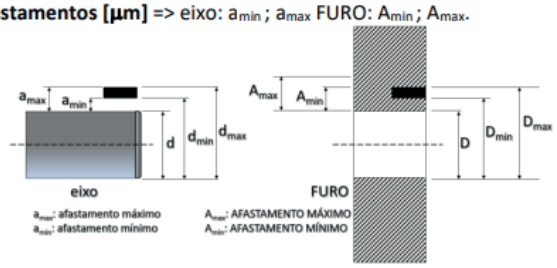

Interferências [µm]=> Z: real (pós-montagem); I: inicial (pré-montagem); ΔI: perda de interferência na montagem. Ra: rugosidade superficial média [µm].

$$Z_{min} = I_{min} - \Delta I = a_{min} - A_{max} - \Delta I$$

$$Z_{max} = I_{max} - \Delta I = a_{max} - A_{min} - \Delta I$$

Obs.: a eventual perda de interferência (ΔI) depende do tipo de montagem.

Montagem axial forçada por prensagem com velocidade controlada ($\Delta I \neq 0$)

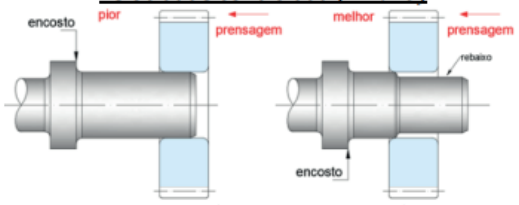

$$\Delta I = 1{,}2 \cdot (Ra_{CUBO} + Ra_{eixo})$$

$$F_m \geq 0{,}7 \cdot \pi \cdot 0{,}5 \cdot \mu \cdot k \cdot d \cdot L \cdot p_{max}$$

$$F_d \geq \pi \cdot \mu \cdot k \cdot d \cdot L \cdot p_{max} \quad ; \quad \mu_D = 0{,}5 \cdot \mu$$

Forças [N]=> F_m: montagem; F_d: desmontagem

μ: coeficiente de atrito estático [adimensional]

μ_D: coeficiente de atrito dinâmico [adimensional]

k: coeficiente de segurança para a fase de montagem ou desmontagem [adimensional]

L: comprimento útil do contato no qual ocorre a interferência entre o CUBO e o eixo [mm]

Montagem radial por dilatação térmica ($\Delta I = 0$)

$$T_m = T_{amb} + \frac{I_{max} \cdot 10^{-3} + 5 \cdot 10^{-4} \cdot d}{\alpha \cdot d} \qquad \Delta T = T_m - T_{amb}$$

Temperaturas [°C]=> T_m: montagem; T_{amb}: ambiente; ΔT: variação de temperatura necessária para a montagem radial.

d: diâmetro nominal [mm]; I_{max}: interferência máxima [µm]

α: coeficiente de dilatação térmica [$°C^{-1}$]

Montagem		Prensagem axial				Dilatação radial			
Eixo		Aço				Aço			
Cubo		Aço	FoFo	Alumínio	Latão	Aço	Aço	FoFo	Alumínio
Lubrificação		óleo	óleo	seco	seco	óleo	seco	seco	seco
μ	mín.	0,05	0,07	0,02	0,03	0,08	0,07	0,07	0,05
	máx.	0,17	0,12	0,06	0,06	0,17	0,19	0,16	0,06

R_a [µm]	desbaste	médio	acabamento	
			fino	finíssimo
Simbologia	∇	∇∇	∇∇∇	∇∇∇
Classe ISO	N9-N10	N7-N8	N7-N8	N1↔N6
torneamento	16 a 40	x	6 a 16	3 a 6
fresamento	12 a 32	x	8 a 15	4 a 8
furação	10 a 25	6 a 10	3 a 6	x
retificação	16 a 40	6 a 16	3 a 6	1 a 3
brochamento	x	x	2 a 4	x

$$p_{min} = \frac{Z_{min} \cdot 10^{-3}}{(K_i + K_e) \cdot d_{eixo}} \qquad K_i = \frac{1}{E_i} \cdot \left(\frac{1 + Q_i^2}{1 - Q_i^2} - \nu_i\right) \;;\; Q_i = \frac{d_i}{d_e} \;;\; K_e = \frac{1}{E_e} \cdot \left(\frac{1 + Q_e^2}{1 - Q_e^2} + \nu_e\right) \;;\; Q_e = \frac{D_i}{D_e}$$

$$p_{max} = \frac{Z_{max} \cdot 10^{-3}}{(K_i + K_e) \cdot d_{eixo}}$$

E: módulo de elasticidade axial [MPa]. ν: coeficiente de Poisson [adimensional].

Fatores elásticos [MPa^{-1}] => K_i: eixo; K_e: CUBO

Fatores geométricos [adimensional]=> Q_i: eixo; Q_e: CUBO

Pressão mínima entre CUBO e eixo [MPa]: p_{min}

Pressão máxima entre CUBO e eixo [MPa]: p_{max}

Escorregamento: $f_{at} \geq R$

$$\pi \cdot \mu \cdot d \cdot L \cdot p_{min} \geq \sqrt{F_a^2 + \left(\frac{2 \cdot T}{d}\right)^2}$$

Forças [N] => f_{at}: atrito; R: resultante.

Interferências reais [μm]: Z (Z_{max} ou Z_{min}).

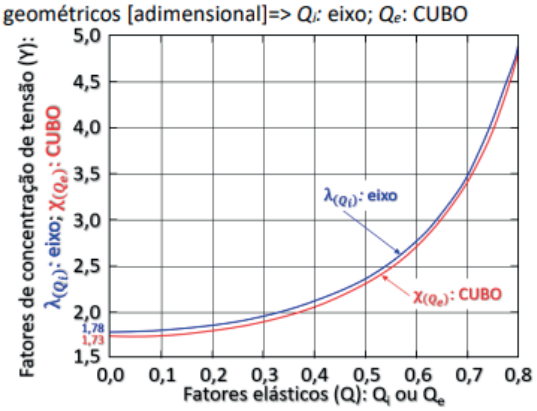

Fatores de concentração de tensão Y=> $\lambda_{(Q_i)}$: eixo; $\chi_{(Q_e)}$: CUBO

Esmagamento: $p_{atuante} \leq p_{adm}$

eixo: $p_{max} \cdot \lambda_{(Q_i)} \leq \frac{\sigma_{e_{eixo}}}{n_{mec_{eixo}}}$

CUBO: $p_{max} \cdot \chi_{(Q_e)} \leq \frac{\sigma_{e_{CUBO}}}{n_{mec_{CUBO}}}$

Coeficiente de segurança de esmagamento => n_{mec}

The professor maintains a YouTube channel where the courses he teaches are presented in playlists. During the lectures, the theory underlying the physical phenomena is explained, and all mathematical deductions are presented. For more information, please visit: https://www.youtube.com/channel/UCeRILnon_gofsbBvT3YDFPg